Quaternary Science Reviews
March 2017, Volume 159 Pages 139-154
https://doi.org/10.1016/j.quascirev.2017.01.020
https://archimer.ifremer.fr/doc/00371/48205/

Large-scale response of the Eastern Mediterranean thermohaline circulation to African monsoon intensification during sapropel S1 formation

Tesi T. [1, *], Asioli A. [2], Minisini D. [3], Maselli V. [4], Valle G. Dalla [1], Gamberi F. [1], Langone L. [1], Cattaneo Antonio [5], Montagna P. [1], Trincardi F. [1]

[1] CNR, CNR ISMAR, Ist Sci Marine, Via Gobetti 101, I-40129 Bologna, Italy.
[2] CNR, IGG, Via G Gradenigo 6, I-35131 Padua, Italy.
[3] Shell Int Explorat & Prod Inc, 3333 Highway 6 South, Houston, TX 77082 USA.
[4] Univ Aberdeen, Dept Geol & Petr Geol, Kings Coll, St Marys Bldg, Aberdeen AB24 3UF, Scotland.
[5] IFREMER, Geosci Marines EDROME, Ctr Brest, BP70, F-29280 Plouzane, France.

* Corresponding author : T. Tesi, email address : tommaso.tesi@bo.ismar.cnr.it

Abstract :

The formation of Eastern Mediterranean sapropels has periodically occurred during intensification of northern hemisphere monsoon precipitation over North Africa. However, the large-scale response of the Eastern Mediterranean thermohaline circulation during these monsoon-fuelled freshening episodes is poorly constrained. Here, we investigate the formation of the youngest sapropel (S1) along an across-slope transect in the Adriatic Sea. Foraminifera-based oxygen index, redox-sensitive elements and biogeochemical parameters reveal – for the first time – that the Adriatic S1 was synchronous with the deposition of south-eastern Mediterranean S1 beds. Proxies of paleo thermohaline currents indicate that the bottom-hugging North Adriatic Dense Water (NAdDW) suddenly decreased at the sapropel onset simultaneously with the maximum freshening of the Levantine Sea during the African Humid Period. We conclude that the lack of the “salty” Levantine Intermediate Water hampered the preconditioning of the northern Adriatic waters necessary for the NAdDW formation prior to the winter cooling. Consequently, a weak NAdDW limited in turn the Eastern Mediterranean Deep Water (EMDWAdriatic) formation with important consequences for the ventilation of the Ionian basin as well. Our results highlight the importance of the Adriatic for the deep water ventilation and the interdependence among the major eastern Mediterranean water masses whose destabilization exerted first-order control on S1 deposition.

Highlights

► The Adriatic S1 is coeval with the Eastern Mediterranean S1 deposits. ► The Adriatic S1 onset is synchronous with the shutdown of the NAdDW. ► African monsoons weakened the LIW which in turn hampered the NAdDW formation.

Keywords : Sapropel S1, Mediterranean sea, African monsoons, Anoxia, Thermohaline circulation

1. Introduction

Periodic perturbations of marine ecology and geochemistry have occurred in the eastern Mediterranean Sea (EMS) since the late Miocene (Nijenhuis et al., 1996). Signs of these changes are preserved in the sediment record as organic carbon-rich deposits commonly known as sapropels. In this study we focus on the most recent sapropel (S1) which formed during the last post-glacial eustatic rise (ca. 10-6 cal kyr BP (De Lange et al., 2008; Hennekam et al., 2014; Schmiedl et al., 2010). It is now largely accepted (Rohling et al., 2015) that favourable conditions for S1 formation were associated with anoxic bottom waters that developed during periods of insolation maxima (Hilgen, 1991; Rossignol-Strick, 1985; Rossignol-Strick et al., 1982). The resulting effect of these orbital variations was the northward migration of the African monsoons resulting in higher precipitation over the Nile river watershed which in turn enhanced the freshwater supply to the ~~EMS~~ southeastern Mediterranean Sea (Hennekam et al., 2014; Weldeab et al., 2014). In addition, the mid-Holocene increase of river runoff from northern borderlands and the post-glacial inflow of less saline Atlantic waters have further contributed to maintaining reduced surface water salinities and high nutrient concentrations in the euphotic zone (Grimm et al., 2015; Kotthoff et al., 2008; Spötl et al., 2010; Toucanne et al., 2015). To date, whether and to what degree either water stratification or enhanced primary productivity has resulted in anoxic bottom waters is still a matter of debate despite several decades of extensive study (Calvert et al., 1992; De Lange et al., 2008; Grimm et al., 2015; Sachs and Repeta, 1999).

A survey of the current literature dealing with S1 reveals that most of the focus has been placed on south-eastern Mediterranean sediments while the Adriatic Sea – that today plays a first-order control on Eastern Mediterranean ventilation (Klein et al., 2000) – has received markedly less interest. In particular,

it has been suggested (Rohling et al., 1997; Rohling et al., 2015) that the onset of critical oxygen conditions in the Adriatic (ca. 8.8 cal. ky BP) lagged behind the fairly synchronous anoxia which developed over the rest of the EMS (ca. 10 cal. ky BP) (De Lange et al., 2008; Schmiedl et al., 2010). This implies that the ventilation regime under which the Adriatic sapropel formed must have been necessarily different compared to the south-eastern Mediterranean sapropels. In particular, it was inferred that persistent ventilation in the Adriatic during the early stage of ~~the~~ sapropel formation hampered the initial development of oxygen-depleted conditions justifying the delayed S1 onset in respect to the rest of the EMS (Mercone et al., 2000; Rohling et al., 2015).

This high-resolution (decadal-~~millennial~~centennial) study aims at testing this hypothesis by reconstructing the oceanographic regime under which Adriatic sapropels formed. ~~-~~Our analysis builds on three well-dated sediment cores collected in three different water depths from the shelf to the deep basin (Fig. 1 and 2). With the objective of understanding timing and conditions which promoted anoxic bottom waters, we present a suite of complementary analyses which include foraminifera assemblages, inorganic elemental composition and organic matter composition. The relatively young age of S1 makes it an ideal target to develop a precise radiocarbon-based Bayesian age model across the three sites establishing also a robust chronological link to other S1 ~~depostis~~deposits across the EMS. Thus, by identifying coeval and genetically linked ~~deposits~~strata, we will evaluate the necessary conditions leading to the sapropel S1 formation in Adriatic sediments and test to what extent these prerequisites are linked to the deposition of sapropel beds in the rest of the EMS.

2. Material and methods

2.1 Sediment cores

The dataset presented here consists of three piston cores retrieved in the Adriatic Sea with variable barrel lengths (5–20 m) (Fig.1 and 2). Core AMC99-1 (45°51'.80 N & 14°45'.68 E, 260 m; Fig. 1) was collected in the central Adriatic basin from the bottom of the mid-Adriatic depression (MAD, Fig. 2b).

Core INVAS12-10 (41°30'.25 N & 17°10'.78 E, 570m; Fig 3) and core SA03-1 (41°30'.25 N & 17°10'.78 E, 567 m) were collected 5 m apart from each other (i.e., twin cores; Fig. 1 and 2c) in the southwest Adriatic slope. Finally, core ST04-1 (41°27'.46 N & 17°31'.05 E, 1085 m; Fig. 3) was retrieved in the deep basin plain of the south-western Adriatic Sea (Fig. 1 and Fig. 2c).

2.2 Seismic acquisition ~~and core handling~~

The seismic dataset used in this study has been collected by ISMAR-CNR (Bologna) on board R/V Urania, in the last two decades. Seismic data were acquired with a hull-mounted Chirp-Sonar Profiler with 16 transducers, characterized by 2–7 kHz sweep-modulated bandwidth, equivalent to a 3.5 kHz profiler, with a recording length up to 1500 ms, depending on water depth, and a penetration of 50–100 m, with vertical resolution of ca. 0.5 m. Track line positioning was based on differential GPS navigation, assuring a position accuracy of 10 m and transformed to geographic coordinates referred to the ED-50 datum.

2.3 Digital x-ray radiograph

Prior to subsampling, cores were x-rayed using a Gilardoni MPX160 as a source and an amorphous 30 cm long silicon (a-Si) flat panel sensor as a detector (Kodak) typically exposed at 70 kV and 5 mA for ca. 6.4 s. For each digital image the pixel dimension is 125 μm and resolution is 1932×2348 pixels.

2.~~3~~ 4 Foraminifera

Sediment samples (1-cm thick interval) were oven dried at 50°C, washed through a 63 μm sieve and dried again at 50°C. Each sample was subsequently split into aliquots using a Jones microsplitter. Aliquots were counted to reach at least 300 specimens of planktonic foraminifera and 300 specimens of benthic foraminifera. In anoxic beds only planktonic foraminifera were observed. The quantitative study was performed on the fraction >10~~60~~μm to avoid juvenile specimens, consistent with the existing Adriatic

literature (Favaretto et al., 2008; Narciso et al., 2012; Piva et al., 2008). However, the <1~~6~~06 μm fraction was always checked in order to identify those specimens which can pass the mesh because of an elongated shape of their shell (e.g. *Fursenkoina*) or because of the small size of their adult stage (e.g. *Epistominella*).

~~-~~Foraminifera concentration is reported as the number of specimens per gram of dry sediment. Data were then integrated with previous published studies (core SA03-1 and AMC99-1; (Favaretto et al., 2008; Narciso et al., 2012; Piva et al., 2008)) to gain higher resolution within the time interval studied. Specifically, twenty-two new samples from SA03-01 were merged with published data (Favaretto et al., 2008; Narciso et al., 2012) while 42 new samples from core AMC99-1 were integrated with data published (Piva, 2007; Piva et al., 2008). Finally, fifty-three samples of core INVAS12-10 were examined with a semi-quantitative analysis to identify key levels (bioevents) for stratigraphic and chronologic purposes (i.e., correlation with the sister core SA03-1), as all geochemical analyses were performed on core INVAS12-10.

The Oxygen Index (OI) (Schmiedl et al., 2003) was used to provide a general trend of bottom oxygen conditions. It is calculated as (HO/(HO+LO)+Div) x 0.5 where HO is the relative abundance of high oxygen indicators (Miliolids, *Articulina tubulosa+Cibicidoides pachydermus+Gyroidinoides orbicularis*), LO is the relative abundance of low oxygen indicators (*Fursenkoina* spp., *Chilostomella oolina*, *Globobulimina* spp.), and Div is the normalized benthic foraminiferal diversity H(S). The term is multiplied by 0.5 to distinguish between anoxic (minimum value = 0) and oxic (maximum value = 1) conditions (Schmiedl et al., 2010; Schmiedl et al., 2003). The index has been calculated for cores ST04-1 and SA03-1, while for core AMC99-1 the term LO (=species of the group A by (Jorissen, 1999) with a deep infaunal microhabitat, especially resistant to low oxygen conditions), has been replaced by the infaunal benthonic taxa of the group B by Jorissen (1999), that is *Bolivina* spp/*Brizalina* spp, *Bulimina costata/ inflata* and *Uvigerina peregrina*, with an infaunal microhabitat, more opportunistic than the species of group A , but less resistant for low oxygen conditions (Schmiedl et al., 2003) because deep infaunal species were absent, or near-absent, during the time equivalent to the Sapropel 1a deposition, as

already reported in the central Adriatic by Ariztegui et al. (2000). The absence/near-absence of species of the LO term would have resulted into not realistic values indicating highly oxygenated bottom condition in the OI index during the Sapropel 1a interval, making necessary the use of the abundant taxa of group B.

Reworked species used as bottom current proxy include the modern living inner-shelf species such as *Ammonia* spp, *Elphidium* spp, *Haynesina* spp. and epiphyitic species (*Asterigerinata* spp, *Buccella granulata*, *Patellina corrugata*) (Jorissen, 1988) corresponding to Biofacies II and III in the Adriatic. We interpret the presence of these displaced species by sediment shedding from shallower waters (Trincardi et al., 2007), in particular from outer-shelf coarser/sandy (Spagnoli et al., 2010) deposits formed during the LGM and presently swept by NAdDW. ~~The Oxygen Index (Schmiedl et al., 2003) has been calculated for cores ST04-1 and SA03-1, while for core AMC99-1 the term LO (=low oxygen indicators, corresponding to the deep infaunal benthonic species (Jorissen, 1999)) has been replaced by infaunal benthonic species (*Bolivina* spp/*Brizalina* spp, *Bulimina costata/in*flata and *Uvigerina peregrina*) (Schmiedl et al., 2003) as deep infaunal species were absent.~~ Reworked species used as bottom current proxy include *Ammonia* spp, *Elphidium* spp, and ~~epifitic~~epiphytic species corresponding to Biofacies II and III in Adriatic (Jorissen, 1988). ~~We interpret the presence of these displaced species by sediment shedding from shallower waters (Trincardi et al., 2007), in particular from outer-shelf coarser/sandy (Spagnoli et al., 2010) deposits formed during the LGM and presently swept by NAdDW.~~

~~Reworked species used as bottom current proxy include the modern living inner-shelf species such as *Ammonia spp, Elphidium spp, Haynesina spp. and epifitic species* (*Asterigerinata spp, Buccella granulata*, *Patellina corrugata*) (Jorissen, 1988) corresponding to Biofacies II and III in the Adriatic. We interpret the presence of these displaced species by sediment shedding from shallower waters (Trincardi et al., 2007), in particular from outer-shelf coarser/sandy (Spagnoli et al., 2010) deposits formed during the LGM and presently swept by NAdDW.~~

Radiocarbon measurements on monospecific tests (5-7 mg) of the planktonic foraminifer *Globigerinoides ruber* (species living above the thermocline) were performed at the National Ocean

Sciences Accelerator Mass Spectrometry (NOSAMS) Facility (USA). On average, 400-600 specimens were hand-picked from the size fraction > ~~0.~~180 µ~~m~~m. Specimens were ultrasonicated in distilled water to remove potential sediment impurities. For level ST040-1 XII 61-62 cm, the planktonic foraminifer *Globorotalia inflata* was used due to the lack of a sufficient amount of *G. ruber* specimens.

2.~~6~~ 5 X-ray fluorescence (XRF)

The inorganic composition of bulk sediments was characterized using a wavelength dispersive sequential Philips PW2400 XRF spectrometer (Mercone et al., 2001) (~~at the~~ Department of Geosciences, (~~(~~University of Padova). The XRF instrument was operated under vacuum conditions on samples prepared as glass beads using lithium tetraborate and melted with a fluxer Claisse Fluxy (~1150°C). The standard error (based on several measurements of the same sample) is less than 0.6% and 3% for major element and trace elements, respectively. For this study, we focused on selected elements which include Ti, V, Mn and S. ~~. Sediments corresponding to tephra layers (characterized by high Zr excess) were analyzed but the data are not shown.~~

2.~~7~~ 6 Grain-size

About 3 g of dried sediments were resuspended in a 40 ml solution of sodium metaphosphate (0.6%) and sonicated for 20 minutes at high energy. Prior to the analysis, sample~~sd~~ were wet sieved at 63 µm. A few drops of wet samples were checked with the microscope to examine the presence of microfossil remains. ~~P~~Particle size distribution of the <63 µm fraction was measured using a Micromeritics SediGraph™ III 5120~~.~~ according to the settling velocity method (Bianchi et al., 1999). Sortable silt concentration was calculated as the fraction by weight of the total mass ranging between 10 and 63µm (McCave and Hall, 2006).

2.~~8~~ 7 Organic Geochemistry

Samples for organic carbon (OC) content were placed in silver capsules and pre-treated with HCl (1.5 M) to remove the inorganic carbon (Nieuwenhuize et al., 1994). Oven-dry samples were analysed using a Thermo Quest-Finnigan Delta Plus isotope ratio mass spectrometer, directly coupled to a FISONS NA2000 Elemental Analyzer by means of a CONFLO II interface.

Lignin analyses (terrigenous biomarkers) were carried out using a Microwave digestion system (Tesi et al., 2014). Dry samples were placed in Teflon vessels with 8 ml of alkaline solution (2N NaOH), 500 mg of CuO, 50 mg of $Fe(NH_4)2(SO_4)2{\cdot}6H_2O$ and oxidized for 1.5 h at 150 °C. After the oxidation, a known amount of recovery standards (ethylvanillin and trans-cinnamic acid) were added to each vessel and acidified to pH 1 with HCl. Reaction products were then extracted with ethyl acetate, evaporated to dryness under N_2 and redissolved in pyridine. Reaction products were analysed as trimethylsilyl derivatives (BSTFA reagent) via GC-MS. Compounds were separated chromatographically in a 30 m×250 µm DB1 (0.25 µm film thickness) capillary GC column, using an initial temperature of 100 °C, a temperature ramp of 4 °C min^{-1} and a final temperature of 300 °C. Phenol biomarkers were quantified using the response factors of commercially available standards (Tesi et al., 2014).

3. Chronology

3.1 Age-depth models

Bayesian age-depth models were performed using the OxCal 4.2 program (https://c14.arch.ox.ac.uk/embed.php?File=oxcal.html) and a comprehensive dataset, which includes both ^{14}C measurements carried out on monospecific foraminifera samples (this study) as well as radiocarbon-dated bioevents based on a detailed event biostratigraphy from each sediment core (Fig. 4 and 5). Radiocarbon age (uncalibrated) of well-known bioevents was based on published studies in the Adriatic (Table 1).

Bioevents (uncalibrated) used for the age-depth models include the following planktonic species or planktonic assemblage turnovers (Fig. 4 and Table 1):

- Bioevent I (10450±90 ^{14}C yBP), abrupt increase of *Globigerinoides ruber*, a warm-water species ~~signaling~~signalling the top of the Younger Dryas dated in core CM92-43 (Asioli et al., 2001). This bioevent marks the end of the Greenland Stadial 1 (GS1) and the beginning of the Holocene (top ecozone V) (Asioli et al., 2001; Asioli et al., 1999; Blockley et al., 2004) and also the top of ecozone 7 (Siani et al., 2010) . The GS-1/Holocene transition is also testified by the lowering of the δ^{18}O values (Asioli et al., 1999; Jorissen et al., 1993; Narciso et al., 2012; Siani et al., 2000);

- Bioevents II and III (9860±60 and 9360±50 ^{14}C yBP, respectively), two peaks in the abundance of *Globorotalia inflata* (i.e., younger and older). These bioevents were described and dated in core SA03-1 (Favaretto et al., 2008) before its temporary disappearance at the base of the Sapropel S1;

- Bioevent IV (5880±60 ^{14}C yBP), last Occurrence of *G. inflata* dated in core RF93-30 (Trincardi et al., 1996). This is a well-documented bioevent recognized in the whole Adriatic after the sapropel S1termination (Ariztegui et al., 2000; Asioli et al., 1999; Capotondi et al., 1999; Siani et al., 2010).

All ^{14}C dates (new radiocarbon dates and bioevents) were converted to calendar years (cal yr BP) using the latest Marine13 calibration curve (Reimer et al., 2013) in OxCal, prior to calibration, ages were corrected for an extra 136±41 ^{14}C-years regional reservoir effect (ΔR) using the values reported in the Marine Reservoir Correction Database (http://calib.qub.ac.uk/marine/). Above the sapropel unit (<5 kyr), the age-depth model of AMC99-1 relays on benthic monospecific tests (*Cibicidoides pachyderma*). For this reason, ~~Only for core AMC99-1 and above the sapropel deposit, ΔR was set 336±41~~ an extra 200 years of reservoir correction was used for these ~~for~~ radiocarbon ages ~~*Cibicidoides pachyderma* (benthic species) based~~ according to ~~on~~ the ~~difference~~ offset between planktonic and benthonic organisms previously assessed in this core (Piva et al., 2008). Bayesian age-depth model (Lowe et al., 2007; Ramsey, 1995; Ramsey and Lee, 2013) was implemented using variable rigidity for the Poisson-Process Modeling (*k* variable ranging between 0.01 and 100 cm^{-1}). The Outlier-Model analysis was performed with the

General setting and the prior probability fixed to 0.05, which weighs down the radiocarbon measurement that have statistical probability of more than 5% of being outliers. The output resulted in robust age models with an overall solid structure of the dated sequence (Fig. 5) as defined by an excellent agreement index (>90%) between calibrated and modelled ages.

It is worth mentioning that foraminifera assemblages were studied in SA03-1 core while the rest of the analyses were performed on the sister core INVAS12-10 from the same site (Fig. 1 and 2c) on which we have constructed the age-depth model based on a greater number of radiocarbon measurements. Cross-correlation between twin cores was carried out relaying on bioevents and tephra (magnetic susceptibility anomalies). Events in chronological order include: top of the Younger Dryas, two *G. inflata* peaks (during the Pre Boreal), peak of *C. bradyi*, a large magnetic susceptibility peak marking a tephra layer, two *G. inflata* peaks (during S1 break and S1b, respectively) and the Llast Occurrence of *G. inflata* (Fig. 4). Ages between midpoints were estimated via linear interpolation.

~~**3.2. Comparison between stratigraphic records from the southern Adriatic basin**~~

~~Prior studies have investigated the S1 in the southern Adriatic basin in the following cores: IN68-9 (Jorissen et al., 1993; Rohling et al., 1997; Van Straaten, 1970), MD90-197 (Mercone et al., 2001; Mercone et al., 2000; Siani et al., 2013; Siani et al., 2000; Siani et al., 2010) and AD91-17 (Capotondi et al., 1999; Giunta et al., 2003; Sangiorgi et al., 2003) (Fig. 6A). Here, prior to presenting and discussing the data, we compare our record from the same region with these published records from the stratigraphic point of view. For the comparison, we selected five main widespread bioevents commonly observed in the Adriatic Sea (Fig. 6B) (Asioli et al., 1999; Narciso et al., 2012; Piva et al., 2008; Rohling et al., 1997; Santacroce et al., 2008; Trincardi et al., 1996). Bioevents include:~~

~~- bioevent I (top GS-1/YD): abrupt increase of *G. ruber*~~
~~- bioevent II: older peak of *G. inflata*~~
~~- bioevent III: younger peak of *G. inflata*~~

- *G. ruber* maximum peak of frequency in S1a

- *Globoturborotalita rubescens* peak in S1a

Among these cores, IN68-9 core (i.e., core 362 in previous publications (Van Straaten, 1970) is particularly relevant because our current understanding of the S1 onset is largely based on this record (Rohling et al., 1997; Rohling et al., 2015). IN68-9 was collected at 1234 m water depth (Fig. 11A) and all the aforementioned biostratigraphic events (source PANGEA, doi:10.1594/PANGAEA.407648) are present and stratigraphically coherent with ST04-1 (bioevent I corresponds in this core to the ecozones I/II boundary) (Fig. 6B). Another similarity includes the ash layer at cm 128-130. Geochemical analysis defined this event as Mercato tephra (Calanchi and Dinelli, 2008) which is positioned just below the increase of *G. rubescens*.

Despite the overall coherence between IN68-9 and ST04-1 from a stratigraphy point of view, bioevents in IN68-9 exhibit a much younger age compared ST04-1, especially within S1a. To further investigate this discrepancy, we performed a new picking of planktonic foraminifera directly on IN68-9 close to the *G. ruber* peak (137-138 cm). It was possible to date this interval in core IN68-9 because two-thirds of the original core are currently stored at ISMAR Bologna. The new radiocarbon date (9030±30 yr BP, uncalib.; NOSAMS-WHOI; Table S1) turned out much older than the age assessed with the previous age-depth model (ca. 8110 yr BP ^{14}C age) but remarkably consistent with the chronology of ST04-1.

The reason for this offset (ca. 1000 y) between the new radiocarbon date and the previous age-depth model (Rohling et al., 1997) is unknown and falls outside the scope of this manuscript. However, it is worth mentioning that the age-depth model of IN68-9 within the S1 interval essentially relies only on two radiocarbon dates (Rohling et al., 1997). We can only suppose that the problem might derive from the lowest radiocarbon date (155.5-157.5 cm, 9280±180 yBP ^{14}C) which is somehow erroneously too young. In fact, this interval roughly corresponds to bioevent II which is again much younger (ca. 1000 years) when compared with our record. Furthermore, this offset is conservative considering that this radiocarbon

test at 155.5-157.5 cm corresponds to a mixture of benthic foraminifera (Jorissen et al., 1993). Thus, at most, the radiocarbon date should have been older rather than younger.

Core MD90-197 was collected at 1010 m water depth (Fig. 6A). Three curves of planktonic species (*G. ruber*, *G. inflata* and *Globigerinita glutinata*) were visually extrapolated based on the plot of planktonic species *vs* age previously published (Siani et al., 2010). For this core only two bioevents of core ST04-1 were recognized: Bioevent I and II. The *G. ruber* peak is present but it is coeval with the tephra layer E1 (Gabellotto-Fiumebianco) located close to the S1 interruption and proved to be younger than Mercato tephra (Caron et al., 2012; Marchini et al., 2014). What is striking about this core is the relatively lower thickness of S1a compared to S1b which is unusual for S1 (Mercone et al., 2001; Mercone et al., 2000). This might reflect either a condensed interval or a hiatus above the *G. glutinata* peak. To test this hypothesis, we compared the V/Al record that displays a large peak right after the S1 onset in both Adriatic basin (ST04-1) and slope (INVAS12-10) (Fig 6C). This peak is also well present in other south-eastern S1 deposits (e.g., LC21, Aegean Sea (Mercone et al., 2001). The XRF analyses were performed every cm in MD90-197. However, despite the high resolution, the V/Al peak is not visible (Mercone et al., 2001) (Fig. 12C)

An examination of all radiocarbon dates available for MD90-197 (both mixed planktonic foraminifera and monospecific tests (Mercone et al., 2000) reveals a drastic drop in sedimentation rate where the V/Al is expected. This suggests once again either a condensed unit or a hiatus. Even considering the error associated with pulling together monospecific radiocarbon tests and mixed planktonic species (these latter integrate the signal of a thicker water column), the apparent drop of sedimentation seems to be still evident in the radiocarbon data (Mercone et al., 2000). Unfortunately, benthic foraminifera are not available for MD90-197 which hampers the direct comparison with ST04-1. For example, the *C. bradyi* observed in both ST04-1 and IN68-9 at the base of S1a could have provided additional important clues.

Finally, core AD91-17 was collected at 844 m water depth. Two curves of planktic foraminifers (*G. ruber* and *G. inflata*) were reported in Fig. 6A based on previous studies (Capotondi et al., 1999). A recent study

~~showed that the Mercato tephra in this core is present in correspondence of the S1 onset (Marchini et al., 2014). However, Mercato is stratigraphically positioned ca. in the middle of S1a above the *G. ruber* peak in both IN68-9 and ST04-1, this implies that the lower part of S1a is not present. Indeed, just below Mercato, previous publications have highlighted the presence of a turbidite (Giunta et al., 2003).~~

~~Finally, core AD91-17, collected at 844 m water depth (6A), records the Sapropel 1 deposition between cm 190 and 125 (Giunta et al., 2003, Marchini et al., 2014). Two curves of planktic foraminifers (G. ruber and G. inflata) were reported in Fig. 6A based on previous studies (Capotondi et al., 1999). Tephrostratigraphy of this core shows that the sapropel onset (190-191 cm) corresponded to upper limit of Mercato tephra (Marchini et al., 2014). However, Mercato tephra is stratigraphically positioned ca. in the middle of S1a, above the *G. ruber* peak in IN68-9 (Calanchi and Dinelli, 2008; Rohling et al., 1997) and in ST04-1. The fact that this *G. ruber* positioned peak below Mercato is not visible in AD91-17 (Fig. 6A) suggests that the lower portion of the S1a is missing. In fact, previous publications have highlighted the presence of a turbidite just below Mercato between cm 200 and 196 (Giunta et al., 2003) which further support the hypothesis of the stratigraphic gap.~~

4. Results and discussion

4.1 Coeval sapropel deposits cross-margin settings

In this study we present data from sediment cores retrieved in three different regions of the Adriatic Sea: (i) the mid-Adriatic depression (MAD), (ii) the south-western continental slope and (iii) the southern deep basin (Figs. 1 and 2). The mid-Adriatic depression represents a small remnant basin, which was partially filled with sediment during the last glacial maximum (core AMC99-1, 260 m (Piva et al., 2008); Fig. 2b). High-resolution chirp-sonar profile across the coring site shows continuous and high-amplitude sub-parallel reflectors, which denote sedimentation in low-energy conditions.

The slope coring site is characterized by large-scale bottom-current deposits formed by prolonged activity of the thermohaline circulation (core INVAS12-10 and SA03-1, from 570 and 567 m respectively (Minisini et al., 2006) (~~;~~ Fig. 2c). On chirp profiles, these deposits are organized in fields of large sediment waves characterized by wavy and high-amplitude reflectors (Fig. 2c). The coring site was selected on the depositional (up-current) flank of one sediment wave.

Finally, the coring site in the southern Adriatic deep basin is characterized by pelagic sedimentation as shown by sub-parallel reflectors, although dense NAdDW can occasionally reach and impact this area (ST04-1, 1085 m Minisini et al. (2006); Fig. 2d).

Despite the different bathymetric contexts, radiocarbon dates from monospecific tests indicated that these three records represent coeval deposits within the time interval under examination (Table 1). Detailed biostratigraphy examination for all three cores revealed the occurrence of bioevents commonly observed in the study region, which were used to independently test the stratigraphic continuity of our records (Fig. 4). High-resolution Bayesian ^{14}C-based age-depth models confirmed continuous deposition consistent with bioevents and seismic profiles (Fig. 5).

4.2 Adriatic Sapropel deposition

4.2.1 Pre-sapropel and S1 onset

Sapropels are beds with elevated organic carbon (OC) content that contrast with overlying and underlying sediments. In this study, S1 boundaries are defined based on the OC anomalies in respect to the background level. The definition of sapropels can further extend to anomalies of several other parameters including Ba/Ti ratio, redox sensitive elements, foraminifera assemblages and magnetic susceptibility or simply changes in sediment colour (De Lange et al., 2008; Mercone et al., 2000; Rohling et al., 1997; Santvoort et al., 1997; Schmiedl et al., 2010; Tachikawa et al., 2015; Vigliotti et al., 2008). Here, we will also discuss these other parameters alongside ~~along~~ the OC data in order to provide a multifaceted view on S1 formation.

Our deepest ~~water~~ record ~~in~~ from the southern Adriatic (ST04-01, 1085 m; Fig. ~~7a~~6a) shows a gradual OC increase since 11 cal. ky BP before the typical sapropel onset (ca. 10 cal. ky BP) (Hennekam et al., 2014; Rohling et al., 2015; Schmiedl et al., 2010). This trend is consistent with the foraminifera-based oxygen index (Schmiedl et al., 2010) (OI) which reveals a pre-sapropel deterioration of ~~pore-water~~bottom oxygen levels in the deep basin since ca. 11 cal. ky BP (Fig. ~~8a~~ 7a and Fig. ~~9a~~8a). Analogous pre-sapropel conditions, ascribed to stratification have recently been documented in the deep Levantine basin at 1780 m water depth using a suite of redox-sensitive elements (Tachikawa et al., 2015). Post-glacial freshening driven by the inflow of less saline Atlantic waters via the Gibraltar strait followed by the African Humid Period have certainly exerted a major control on the surface water stratification, vertical mixing and hence intermediate and deep water formation (Rohling et al., 2015; Weldeab et al., 2014). ~~(Rogerson et al., 2008)~~This is ~~also~~ in line with recent regional simulations which described a gradual deterioration of the deep water ventilation in the EMS since the Heinrich-1 event (H1, ca. 18-16 cal ky BP) (Grimm et al., 2015). Enhanced stratification since the H1 event was one of the major drivers that promoted the formation of organic rich layers (ORLs) in the Alboran Sea (Rogerson et al., 2008). In this western Mediterranean region, the continental run-off due to Alpine glacier thawing (i.e., enhanced Rhone river discharge) combined with the Atlantic inflow likely weakened the Western Mediterranean Deep Water ventilation promoting the deposition of ORLs (Rogerson et al., 2008).

The onset of relatively high OC content which marks the beginning of the Adriatic S1 (i.e, S1a) was synchronous among our records and it was dated around 10 cal ky BP ~~in~~ across the ~~all~~ three sites (Fig. ~~7~~ 6 a, b, c). After this coeval OC increase, the deep Adriatic basin (ST04-1) rapidly turned into an azoic environment (Fig. ~~9a~~8a). Specifically, as the pore water oxygen decreased in the basin (Fig. 8a), only infaunal foraminifera could initially tolerate oxygen-poor conditions although the benthic environment rapidly became hostile even for deep infaunal taxa (Fig. ~~9b~~8b). Azoic conditions in the basin are marked also by authigenic vanadium enrichments (V/TiO_2; Fig. ~~9b~~8b) as commonly observed in sapropel beds (Mercone et al., 2001; Tachikawa et al., 2015). Vanadium precipitation is expected in highly reducing environments as its solubility rapidly decreases at the oxic-anoxic boundary which is controlled via

diffusion processes across the sediment-water interface (Mercone et al., 2000). Sulphur enrichment (S/TiO_2) in sapropel beds - likely in the form of authigenic pyrite (Passier et al., 1997) - further corroborates the change of redox conditions characterized by microbial-driven sulfate reduction in response to the oxygen-poor environment (Fig. ~~10~~ 9 d, e, f).

4.2.2 Sapropel break, sapropel S1b and sapropel termination

An interruption within the sapropel unit is visible in our records between ca. 7.8 and 8.3 cal ky BP. During the break both OC content and V/TiO_2 decreased while the OI increased indicating a temporary re-oxygenation at the seabed (Fig ~~7a~~6a, b, c; Fig ~~8~~7). The overall trend observed here has been documented in several other S1 deposits further south-east and down to ca. 1,800 m water depth (De Lange et al., 2008; Tachikawa et al., 2015). Reactivation of the convective overturn driven by heat loss during cooling events in the northern Adriatic has been suggested as the most likely scenario to explain the temporary re-oxygenation (Marino et al., 2009; Rohling et al., 1997). The interruption was particularly evident over basin and slope sediments while in the shallower mid-Adriatic slope basin did not display significant change over the break. Already being an oxic environment, it is likely that the mid-Adriatic depression (AMC99-1) was not particularly affected by the temporary resumption of the ventilation.

After the sapropel break, the second phase of S1 deposition (i.e., S1b) lasted for ca. 1 ky. Both V/Ti ratio and oxygen index indicate that the reducing conditions during S1b were not as severe in slope sediments as during S1a (Fig. ~~8~~ 7 c, d). This is also consistent with the presence of relatively lower authigenic sulphur content, which suggests comparatively lower sulphate reduction rates during S1b (Fig. ~~10~~ 9 d, e, f). By contrast, the deep southern basin became azoic again for ca. 500 yr (Fig. ~~8a~~7 a and 8 a).

The transitory reappearance of benthic foraminifera and high OI value around 7.4 cal ky BP in the deep basin (ST04-1) suggests another short-lived ventilation event within the S1b (Fig. 7~~8~~a) prior to the S1 termination. This was a rather short-lived event but widespread over the EMS as previously observed in the Aegean and Ionian regions (Filippidi et al., 2016).

The complete recovery of the deep-water ventilation, which marks the sapropel termination, was fairly synchronous among our records according to the OC anomalies (ca. 6.8 cal ky BP, Fig. ~~7~~ 6 a,b,c). However, the OI displayed a bathymetric gradient (Fig. ~~8a~~7a, b, c) consistent with what observed in the Levantine and Aegean regions where the ventilation started in shallow environment and gradually extended towards greater water depths ~~towards deeper sediments~~ (Schmiedl et al., 2010). As the oxygen reached the seabed, the authigenic enrichment of MnO_2 (Fig. ~~10a~~9a) provides a geochemical redox marker to track the maximum penetration of oxygen in sediments after the anoxic period (Reitz et al., 2006; Tachikawa et al., 2015).

While OC concentration levels were re-established after the sapropel over basin and slope, the OC remained relatively high in the mid-Adriatic depression (AMC99-1; Fig. ~~7~~ 6 c) even after the S1 termination. The OI based on intermediate infaunal foraminifera reveals a relatively moderate but continuous decrease of the pore-water oxygen concentration in this region throughout the S1 deposition (Fig. ~~8c~~7c). This trend likely reflected the sea level rise which pushed towards land the main path of the North Adriatic Deep Water (NAdDW) causing a less efficient ventilation of the Adriatic depression. It is well documented that the modern NAdDW path is mainly confined to the western shelf due to the Coriolis force as it moves southwards (Vilibić and Supić, 2005). Today, only major events of dense water formation can efficiently ventilate the deepest region of the Adriatic depression (Marini et al., 2015). When this occurs, the dense plume lifts the old water mass which is characterized by relatively low oxygen concentrations testifying its long residence time within the morphological depression (i.e., one or several years) (Marini et al., 2015).

4.3 Sediment waves growth and thermohaline forcing

In the South Adriatic slope within the field of upslope-migrating sediment waves (core SA03-1, 567 m; Fig. 2c), the relative abundance of reworked inner-shelf foraminifera suddenly decreased at the S1 onset (Fig. 6~~7~~d). The presence of allochthonous taxa at this depth is expected considering the

thermohaline forcing that generates these sedimentary bodies (Trincardi et al., 2007). Specifically, sediment waves are essentially swept by protracted thermohaline currents which have sufficient energy to resuspend inner-shelf taxa and disperse them towards greater depths (Langone et al., 2015). Bottom currents in the southern Adriatic slope are principally controlled by LIW and NAdDW as well as their interaction which ultimately generates the Adriatic Eastern Mediterranean Deep Water ($EMDW_{Adriatic}$) (Millot, 1999). Mooring lines deployed just down-flow respect to the sediment wave field showed that the modern NAdDW-driven bottom currents can reach over 60 cm s^{-1} during the cascading season (Langone et al., 2015) (i.e., the modern NAdDW forms around Jan-Feb and reaches the southern margin around March-April (Langone et al., 2015; Turchetto et al., 2007). Consequently, the sudden decrease of inner-shelf taxa coeval with the S1 onset likely reflects the virtual shutdown of the NAdDW or, more precisely, a shallow ventilation confined to the uppermost region of the water column.

This explanation is indeed consistent with the general temporal trend shown by the shedding of allochthonous foraminifera from the shelf throughout the S1 deposition. For example, as previously mentioned, the S1 interruption is likely the expression of a cooling phase which promoted the temporary reactivation of the dense water formation in the northern Adriatic Sea (Rohling et al., 1997) and, consequently, the advection of reworked inner-shelf taxa over the slope (Fig. ~~7d~~6d). Likewise, S1b and S1 termination are associated with decrease and increase of inner-shelf taxa, respectively (Fig. ~~7d~~6d).

The non-cohesive fraction of marine sediments - generally known as ‘‘sortable silt’’ (SS, 10–63 μm) - further supports the decrease of the deep-water ventilation during the S1 deposition (Fig. ~~7e~~6e). The sortable silt is operationally defined as the fraction of fine-grained sediments whose sorting and concentration vary in response to hydrodynamic processes (McCave and Hall, 2006). As large errors affect the SS mean grain estimates for low concentrations of SS, here we report only the SS% by weight as a qualitative proxy for paleo-current regimes (Fig. ~~7e~~6e). The SS% suggests a progressive decrease of the bottom-current energy since the end of the Younger Dryas (ca. 11.5 cal ky BP) with the minimum observed just at the S1 onset. Overall, the SS trend is consistent with the general distribution of the inner-

shelf foraminifera (Fig. ~~7d~~6d), which further highlights drastic changes of the thermohaline forcing associated with the pace of the NAdDW.

4.4 Weakening of LIW as main trigger for Adriatic S1 deposits

Our results from the sediment wave field revealed that the onset of the sapropel S1 in Adriatic sediments is coeval with the drastic weakening of the North Adriatic Deep Water (NAdDW, Fig. 1). Based on this evidence, we envision a direct relation of cause and effect in which suddenly weakened deep water ~~ventilation~~ formation resulted in oxygen depleted bottom waters.

Several combined factors might have caused the abrupt decrease of the thermohaline forcing in the Adriatic Sea. A key aspect to consider lies in the evident similarities with the south-eastern Mediterranean Sea. First of all, the comparison with the Levantine, Aegean and Ionian Seas reveals that the S1 onset in the Adriatic is ~~remarkably~~ coeval (within age-depth model uncertainties) with the sapropel formation in these regions. Specifically, a recent review (Schmiedl et al., 2010) that has compiled several south-eastern Mediterranean cores indicated that the onset of critical oxygen concentrations (i.e, oxygen index being less than 0.5) occurred around 10.2±0.3 cal ky BP. The collapse of the Adriatic benthic fauna in slope and basin sediments based on the same oxygen index threshold occurred within this time interval (Fig. ~~8~~10 ~~a, b~~). This comparison thus reveals that S1 onset in the Adriatic was coeval with the rest of the south-eastern Mediterranean sapropel beds. Further evident similarities ~~with the south-eastern Mediterranean sapropels~~ emerge when comparing the temporal anomalies of several other geochemical parameters such as bulk OC (Filippidi et al., 2016; Hennekam et al., 2014; Vigliotti et al., 2011) and redox-sensitive elements (Filippidi et al., 2016; Hennekam et al., 2014; Mercone et al., 2001; Tachikawa et al., 2015) (notably vanadium).

~~A synchronous S1 onset across the entire EMS – including the Adriatic - is a new element that corrects previous literature which inferred a delayed S1 onset of ca. 1ky in the Adriatic due to protracted ventilation during the early phase of the sapropel formation (Rohling et al., 1997). In the 3.2 section~~

~~(Comparison between stratigraphic records from the southern Adriatic basin) we have further analysed the differences between our results and previous published studies from a stratigraphic point of view. Here we show how time differences are most likely the result of low-resolution age-depth models combined with gravity-driven processes (e.g., erosion, turbidites) which likely altered the original stratigraphy.~~

In light of this new ~~new~~ insight~~information~~, we postulate that the synchronous onset of sapropel S1 over the entire EMS (Fig. 10) necessarily involves the Levantine Intermediate Water (LIW) (Fig. 1~~2~~) which is the binding element of the eastern Mediterranean thermohaline circulation (Millot, 1999). More specifically, we suggest that the most plausible scenario to explain (i) the coeval S1 onset and (ii) the sudden weakening of the NAdDW must be related to the freshening of the south-eastern Mediterranean Sea. According to our hypothesis, because the salty LIW exerts first-order control on the NAdDW formation by pre-conditioning the northern Adriatic waters (Vilibić and Orlić, 2002; Vilibić and Supić, 2005) before the winter cooling, we infer that the freshening of the Levantine Sea during the African Humid Period ~~–~~must have considerably reduced the deep-water formation in the northern Adriatic Sea eventually leading to the deep-water anoxia ~~(Fig. 12b)~~.

To test our hypothesis ~~(Fig. 12b)~~ and in particular the link between the south-eastern Mediterranean region and Adriatic Sea, we have compared our data with a recent reconstruction of the Nile River discharge based on the Ba/Ca ratio measured on *Globigerinoides ruber* (Weldeab et al., 2014) (Fig. ~~7~~f6f). The Ba/Ca record essentially reflects the degree of the freshening of the Levantine surface waters as a function of the African monsoon extent (Weldeab et al., 2014). We found that the maximum freshwater supply to the Levantine Sea (ca. 10 cal ky BP) indeed corresponds to the temporarily NAdDW shutdown (i.e., drop in the inner-shelf taxa and SS, Fig. ~~7~~ 6 d, e) and the corresponding S1 onset in the Adriatic Sea (Fig. ~~7~~ 6 a, b, c and ~~8~~ 7 a, b, c).

Furthermore, considering that the formation of the ~~Adriatic~~ Eastern Mediterranean Deep Water sourced from the Adriatic ~~EMDW~~ ($EMDW_{Adriatic}$) largely depends on the NAdDW (Vilibić and Orlić, 2002; Vilibić and Supić, 2005) (Fig. 1), our results imply that the reduced deep water formation in the

Adriatic had in turn drastically hampered the ventilation of those deep regions under the direct influence of the $EMDW_{Adriatic}$ which today ~~such as the Ionian basin (Fig. 12b). Today the Adriatic~~ represents the major cold and ~~EMDW~~ dense water ~~source~~ of ~~for~~ the EMS (Klein et al., 2000)~~. although under certain climate conditions (commonly known as the Eastern Mediterranean Transient, EMT), the south-eastern surface waters can become particularly salty and generate large volumes of dense water (Lascaratos et al., 1999; Malanotte-Rizzoli et al., 1997). The EMS freshening certainly had important effects on both NAdDW and EMT.~~

Recent studies have also pointed out that ~~that~~ the progressive stagnation of the EMS occurred prior to the African Humid Period due to the inflow of less saline North Atlantic waters into the Mediterranean via the Gibraltar strait (Béthoux and Pierre, 1999; Grimm et al., 2015; Rohling and Bryden, 1994; Rohling et al., 2015). Therefore, the peak of the African monsoon occurred over a period already characterized by enhanced water-column stratification. Evidence of weakened deep-water ventilation prior to S1 has been well documented in the Levantine Basin (Tachikawa et al., 2015)~~15~~, which is consistent with our record in the Adriatic basin (notably ST04-1; Fig. ~~9~~8). The presence of pre-sapropel conditions in our deepest record further highlights the coherence between the Adriatic and the rest of the EMS as well as the importance of pre-freshening as a prerequisite for the sapropel formation (Grimm et al., 2015).

Comment [TT1]:

Among other relevant similarities with the south-eastern Mediterranean sapropels, it is worth mentioning that the S1 termination in the Adriatic was coherent with the progressive reoxygenation observed in the Levantine and Aegean sediments (Fig. 10). Specifically, according to the foraminifera-based oxygen index (values > 0.5) (Schmiedl et al., 2010) in these regions, the ventilation was initially confined within the uppermost water column and gradually increased water depth with time. A similar water depth- trend characterized our Adriatic records. Using the same oxygen-index threshold as for the Aegean and Levantine basins (Schmiedl et al., 2010), the re-oxygenation over the slope (SA03-1, Fig. ~~8b~~7b and 10) occurred ~~much~~ earlier than ~~-~~the deep benthic environment (ST04-1, Fig. ~~8a~~7a and 10). In line with the bottom~~-~~ ~~-~~current proxies (Fig. ~~7~~ 6 d, e), these results suggest a gradual reactivation of the

NAdDW. The reason for the observed bathymetric trend across all Eastern Mediterranean basins probably involves the gradual weakening of the African monsoons (Weldeab et al., 2014) (Fig. ~~7~~6f) coupled with the sea surface cooling towards the end of the sapropel (Marino et al., 2009; Siani et al., 2013).

4.5 Comparison with published stratigraphic records from the southern Adriatic basin

Our results revealed ~~A~~a synchronous S1 onset across the entire EMS which ~~—~~includes ~~ing~~ the Adriatic setting. ~~-~~This~~-~~ is a new element that corrects previous literature which inferred a delayed S1 onset (~~of~~ ca. 1ky) in the Adriatic due to protracted ventilation during the early phase of the sapropel formation (Rohling et al., 1997). ~~In the 3.2~~In this section, we revisit published studies dealing with the Adriatic S1 to evaluate the stratigraphic coherence with our results and, thus, further understand the origin of this discrepancy. ~~section (Comparison between stratigraphic records from the southern Adriatic basin) we have further analysed the differences between our results and previous published studies from a stratigraphic point of view. Here we show how time differences are most likely the result of low-resolution age-depth models combined with gravity-driven processes (e.g., erosion, turbidites) which likely altered the original stratigraphy.~~

Prior Adriatic studies focused on the following cores: IN68-9 (Jorissen et al., 1993; Rohling et al., 1997; Van Straaten, 1970), MD90-197 (Mercone et al., 2001; Mercone et al., 2000; Siani et al., 2013; Siani et al., 2000; Siani et al., 2010) and AD91-17 (Capotondi et al., 1999; Giunta et al., 2003; Sangiorgi et al., 2003) (Fig. 1 and 11). For the comparison with our records, we selected five main widespread bioevents commonly observed in the Adriatic Sea (Fig. 11) (Asioli et al., 1999; Narciso et al., 2012; Piva et al., 2008; Rohling et al., 1997; Santacroce et al., 2008; Trincardi et al., 1996). Bioevents include:

- bioevent I (top GS-1/YD): abrupt increase of *G. ruber*
- bioevent II: older peak of *G. inflata*
- bioevent III: younger peak of *G. inflata*
- *G. ruber* maximum peak of frequency in S1a

- *Globoturborotalita rubescens* peak in S1a

Among these cores, IN68-9 core (i.e., core 362 in previous publications (Van Straaten, 1970) is particularly relevant because our current understanding of the S1 onset is largely based on this record (Rohling et al., 1997; Rohling et al., 2015). IN68-9 was collected at 1234 m water depth (Fig. 11a) and all the aforementioned biostratigraphic events (source PANGEA, doi:10.1594/PANGAEA.407648) are present and stratigraphically coherent with ST04-1 (bioevent I corresponds in this core to the ecozones I/II boundary) (Fig. 11a). Another similarity includes the ash layer at cm 128-130. Geochemical analysis in IN68-9 defined this event as Mercato tephra (Calanchi and Dinelli, 2008) which is positioned just below the increase of *G. rubescens*. Although the geochemical fingerprint is not available for ST04-1, the age and the stratigraphic position suggest that this ash layer is likely Mercato tephra.

Despite the overall coherence between IN68-9 and ST04-1 from a stratigraphy point of view, bioevents in IN68-9 exhibit a much younger age compared to ST04-1, especially within S1a. To further investigate this discrepancy, we performed a new picking of planktonic foraminifera directly on IN68-9 close to the *G. ruber* peak (137-138 cm). It was possible to date this interval in core IN68-9 because two-thirds of the original core are currently stored at ISMAR Bologna. The new radiocarbon date (9030±30 yr BP ^{14}C age.; NOSAMS reference OS-127850; Table 1) turned out much older than the age assessed with the previous age-depth model (ca. 8110 yr BP ^{14}C age) (Rohling et al., 1997) but remarkably consistent with the chronology of ST04-1.

The reason for this offset (ca. 900 y) between the new radiocarbon date and the previous age-depth model (Rohling et al., 1997) might explain why the Adriatic sapropel S1 exhibited a delayed onset. It is worth mentioning that the age-depth model of IN68-9 within the S1 deposit, essentially relies only on two radiocarbon dates (Rohling et al., 1997). Thus, it possible that the problem might derive from the lowest radiocarbon date (UTC-501, 155.5-157.5 cm, 9280±180 yr BP ^{14}C) which is somehow erroneously too young. To test this hypothesis, we re-modelled in Oxcal the sediment accumulation of core IN68-9 using the new radiocarbon date (OS-127850) and the bioevents as used in our records (supplementary material).

The goal of this exercise was to examine the agreement between the model (*prior*) and the observational data (*likelihood*) which is quantitatively expressed with the "agreement index". As expected, test UTC-501 exhibited a low agreement index and, thus, turned out being an outlier. Furthermore, the agreement index would further decrease considering that the suspicious radiocarbon test (UTC-501) corresponds to a mixture of benthic foraminifera (Jorissen et al., 1993). In fact, if we applied a larger ΔR respect to planktonic foraminifera, the new reservoir correction would make the calibrated age even younger and, thus, less coherent with the rest of the dates.

Core MD90-197 was collected at 1010 m water depth (Fig. 1). Three curves of planktonic species (*G. ruber*, *G. inflata* and *Globigerinita glutinata*) were visually extrapolated based on the plot of planktonic species *vs* age previously published (Siani et al., 2010). For this core only two bioevents of core ST04-1 were recognized: Bioevent I and II. The *G. ruber* peak is present but it is coeval with the tephra layer E1 (Gabellotto-Fiumebianco) located close to the S1 interruption and proved to be younger than Mercato tephra (Caron et al., 2012; Marchini et al., 2014). What is striking about this core is the relatively thin S1a compared to S1b which is unusual for S1 (Mercone et al., 2001; Mercone et al., 2000). This might reflect either a condensed interval or a hiatus above the *G. glutinata* peak. To test this hypothesis, we compared the V/Al record that displays a large peak right after the S1 onset in both Adriatic basin (ST04-1) and slope (INVAS12-10) (Fig 11b). This peak is also present in other south-eastern S1 deposits (e.g., LC21, Aegean Sea (Mercone et al., 2001). The XRF analyses were performed every cm in MD90-197. However, despite the high resolution, the V/Al peak is not visible (Mercone et al., 2001) (Fig. 11b). An examination of all radiocarbon dates available for MD90-197 (both mixed planktonic foraminifera and monospecific tests (Mercone et al., 2000) reveals a drastic drop in sedimentation rate where the V/Al is expected. This suggests once again either a condensed unit or a hiatus. Even considering the error associated with pulling together monospecific radiocarbon tests and mixed planktonic species (these latter integrate the signal of a thicker water column), the apparent drop of sedimentation seems to be still evident in the radiocarbon data (Mercone et al., 2000). Unfortunately, benthic foraminifera are not

available for MD90-197 which hampers the direct comparison with our record. For example, the *C. bradyi* observed in both ST04-1 and IN68-9 at the base of S1a could have provided additional important clues.

Finally, core AD91-17 was collected in the southern Adriatic at 844 m water depth (Giunta et al., 2003, Marchini et al., 2014). Two curves of planktonic foraminifera (G. ruber and G. inflata) were reported in Fig. 1 based on previous studies (Capotondi et al., 1999). Tephra-stratigraphy of core AD91-17 indicates that the reconstructed sapropel onset (190-191 cm) corresponded to the uppermost limit of Mercato tephra (Marchini et al., 2014). However, Mercato tephra is stratigraphically positioned ca. in the middle of S1a, above the *G. ruber* peak in both IN68-9 (Calanchi and Dinelli, 2008; Rohling et al., 1997) and ST04-1 (this study). The fact that this large *G. ruber* peak below Mercato is not visible in AD91-17 (Fig. 11a) suggests that the lower portion of the S1a is missing. In fact, previous publications have highlighted the presence of a turbidite just below Mercato between cm 200 and 196 (Giunta et al., 2003) which further support the hypothesis of a possible stratigraphic gap.

4.6~~5~~ Enhanced primary productivity or diagenetic signal?

Alternatively, the deposition of the Adriatic sapropel could have been an expression of the high-nutrient supply via freshwater discharge. Under these circumstances, the increased demand of benthic oxygen, necessary to degrade the freshly deposited marine phytodetritus, eventually resulted in anoxic sediments.

In this study, we used lignin – the second most abundant macromolecule on Earth after cellulose – as a tracer of freshwater discharge because it has been shown that terrestrial organic biomarkers (notably sediment-normalized concentrations) increase during sapropel deposition (Bouloubassi et al., 1999; Gogou et al., 2007) (Fig. ~~11~~12). In northern Mediterranean borderlands, ~~the abundance~~this evidence ~~of terrestrial biomarkers~~ has been widely used to infer the link between enhanced freshwater supply and sapropel formation (Bouloubassi et al., 1999; Gogou et al., 2007). Indeed, our results show that lignin

increased at the S1 onset but, ~~in all settings~~ at the same time, the lignin content markedly diminishes with decreasing water depth (Fig. ~~11~~12). While previous studies mainly drawn their conclusions based on deep sapropel beds (Bouloubassi et al., 1999; Gogou et al., 2007), in this study we took the opportunity to focus also on shallow water equivalent deposits which revealed this water depth trend. However, ~~A~~a pattern like this is~~–~~ unexpected because typically lignin concentration diminishes with increasing distance from the river outlets in all modern continental margins, including the Adriatic (Bröder et al., 2016; Gordon and Goñi, 2003; Tesi et al., 2008; Tesi et al., 2007). Therefore, in our hypothesis, lignin concentration reflects post-depositional degradation efficiency rather than original river input.

In this scenario, early diagenesis during burial is limited in the deep basin where anoxic sediments hamper the complete OC breakdown including the terrestrial fraction. This would explain the relatively high lignin content in the deepest station during S1 as well as the similarities between lignin content and bulk OC (Fig. ~~7~~ 6 a, b, c and ~~11~~12). Taken together, our results indicate that terrestrial biomarkers in sapropel beds do not necessarily reflect a primary signal (river input) but rather a secondary signal (diagenesis) as observed for other "non-conservative" variables measured in sapropel beds~~s~~ such ~~as δ^{15}N,~~ pollen assemblages as well as other organic biomarkers (Cheddadi and Rossignol-Strick, 1995; Langgut et al., 2011; Versteegh et al., 2010). Another recent example is the δ^{15}N whose depleted isotope composition has been interpreted for a long time as a sign of enhanced primary productivity (Calvert et al., 1992). Recent works showed that the lack of isotopic fractionation during early diagenesis is essentially the reason why sapropel beds display depleted δ^{15}N signatures (Möbius et al., 2010; Sachs and Repeta, 1999). Thus, as observed for the terrestrial biomarkers, the δ^{15}N signature in sapropel beds reflects a preservation signal (diagenesis) rather than the original marine OC fingerprint.

Given the evident complications with the use of terrestrial biomarkers we have looked into the literature (Combourieu-Nebout et al., 2013; Magny et al., 2012; Spötl et al., 2010) to find indications of enhanced river discharge from the northern Mediterranean borderlands to justify the sapropel onset at

around 10 cal ky BP. The collective evidence based on speleothems, pollen data and debris flow fans ~~and lake levels~~ suggests precipitation anomalies around ~~7.3~~ 8.2-7.3 cal. ky BP (Spötl et al., 2010; Zanchetta et al., 2007) over the northern ~~Mediterranean~~ Italian drainage basins ~~regions~~ (Alps and northern Apennine chain)~~(i.e., Alps). (Magny et al., 2013)~~The wetter conditions during this period might have further weakened the NADW during the sapropel deposition and stimulated the primary productivity. However, other studies based on lake levels suggest conditions not particularly wet during the same period in northern Italy (Magny et al., 2013). Despite the lack of agreement, ~~(Spötl et al., 2010; Zanchetta et al., 2007)~~it seems evident that this time interval (8.2-7.3 cal. ky BP) (Spötl et al., 2010; Zanchetta et al., 2007) ~~.~~is more ~~which is more~~ consistent with the second phase of sapropel S1 (S1b) rather than ~~its~~ the onset (ca. 10 cal ky BP). In conclusions, there is no evidence in the literature or in our river-proxy data suggesting that S1 in the Adriatic was initiated by enhanced freshwater discharge from local rivers. By contrast, the synchronous onset across the entire EMS suggests a wide-basin, physical-driven mechanism such as the abrupt weakening of the LIW which hampered the dense water formation over the entire Eastern Mediterranean Sea.

Conclusions

This study has redefined the conditions under which the Adriatic S1 formed. Our multifaceted study based on integrated ecological, organic and inorganic parameters indicates that the weakening of the ~~NAdDW~~ Northern Adriatic Deep Water exerted first-order control on the development of anoxic bottom waters in the Adriatic as well as nearby deep basins such as the Ionian Sea. The emerging picture suggests a chain of events in which the intensification of monsoon precipitation over North Africa followed by the weakening of the ~~LIW~~ Levantine Intermediate Water ultimately suppressed the Northern Adriatic Deep Water formation which~~NAdDW leading to the S1 formation in the Adriatic and in those basins further south under~~, consequently, hampered the~~ the direct influence of the~~ Eastern Mediterranean Deep

WaterEMDW$_{Adriatic}$ (e.g. Ionian basin, developmentFig.11). As a result, the expression of the monsoon-fuelled freshening was a synchronous stagnation S1 formation across the entire Eastern Mediterranean Sea including the Adriatic. Finally, our results rule out the increase of nutrient supply as the major driver for the S1 formation in Adriatic sediments.

Acknowledgments

This study was supported by Shell International Exploration and Production Inc. We thank the *R/V* URANIA crew for at sea assistance. This is the ISMAR contribution n. XXXX. We thank Dr. L. Capotondi and Dr. L. Vigliotti for their constructive comments on the first draft of the manuscript. We also thank Dr. Daria Pasqual (University of Padova, Dept. of Geosciences) for her assistance in XRF analyses. We thank two anonymous reviewers and the Editor H. Bauch for their constructive comments. We also acknowledge Prof. Gerhard Schmiedl (Universität Hamburg) and Associate Prof. Syee Weldeab (Earth Science, UC Santa Barbara) for providing published data used in this study.

References

Ariztegui, D., Asioli, A., Lowe, J.J., Trincardi, F., Vigliotti, L., Tamburini, F., Chondrogianni, C., Accorsi, C.A., Bandini Mazzanti, M., Mercuri, A.M., Van der Kaars, S., McKenzie, J.A., Oldfield, F., 2000. Palaeoclimate and the formation of sapropel S1: inferences from Late Quaternary lacustrine and marine sequences in the central Mediterranean region. Palaeogeography, Palaeoclimatology, Palaeoecology 158, 215-240.

Asioli, A., Trincardi, F., Lowe, J., Ariztegui, D., Langone, L., Oldfield, F., 2001. Sub-millennial scale climatic oscillations in the central Adriatic during the Lateglacial: palaeoceanographic implications. Quaternary Science Reviews 20, 1201-1221.

Asioli, A., Trincardi, F., Lowe, J., Oldfield, F., 1999. Short-term climate changes during the Last Glacial–Holocene transition: comparison between Mediterranean records and the GRIP event stratigraphy. Journal of Quaternary Science 14, 373-381.
Béthoux, J.-P., Pierre, C., 1999. Mediterranean functioning and sapropel formation: respective influences of climate and hydrological changes in the Atlantic and the Mediterranean. Marine Geology 153, 29-39.
Bianchi, G., Hall, I.R., McCave, I., Joseph, L., 1999. Measurement of the sortable silt current speed proxy using the Sedigraph 5100 and Coulter Multisizer IIe: Precision and accuracy. Sedimentology 46, 1001-1014.
Blockley, S.P., Lowe, J.J., Walker, M.J., Asioli, A., Trincardi, F., Coope, G.R., Donahue, R.E., 2004. Bayesian analysis of radiocarbon chronologies: examples from the European Late-glacial. Journal of Quaternary Science 19, 159-175.
Bouloubassi, I., Rullkötter, J., Meyers, P.A., 1999. Origin and transformation of organic matter in Pliocene–Pleistocene Mediterranean sapropels: organic geochemical evidence reviewed. Marine Geology 153, 177-197.
Bröder, L., Tesi, T., Salvadó, J.A., Semiletov, I.P., Dudarev, O.V., Gustafsson, Ö., 2016. Fate of terrigenous organic matter across the Laptev Sea from the mouth of the Lena River to the deep sea of the Arctic interior. Biogeosciences 13, 5003-5019.
Calanchi, N., Dinelli, E., 2008. Tephrostratigraphy of the last 170 ka in sedimentary successions from the Adriatic Sea. Journal of Volcanology and Geothermal Research 177, 81-95.
Calvert, S., Nielsen, B., Fontugne, M., 1992. Evidence from nitrogen isotope ratios for enhanced productivity during formation of eastern Mediterranean sapropels.
Capotondi, L., Borsetti, A.M., Morigi, C., 1999. Foraminiferal ecozones, a high resolution proxy for the late Quaternary biochronology in the central Mediterranean Sea. Marine Geology 153, 253-274.
Caron, B., Siani, G., Sulpizio, R., Zanchetta, G., Paterne, M., Santacroce, R., Tema, E., Zanella, E., 2012. Late Pleistocene to Holocene tephrostratigraphic record from the Northern Ionian Sea. Marine Geology 311, 41-51.
Cheddadi, R., Rossignol-Strick, M., 1995. Improved preservation of organic matter and pollen in eastern Mediterranean sapropels. Paleoceanography 10, 301-309.
Combourieu-Nebout, N., Peyron, O., Bout-Roumazeilles, V., Goring, S., Dormoy, I., Joannin, S., Sadori, L., Siani, G., Magny, M., 2013. Holocene vegetation and climate changes in the central Mediterranean inferred from a high-resolution marine pollen record (Adriatic Sea). Climate of the Past 9, 2023-2042.
De Lange, G.J., Thomson, J., Reitz, A., Slomp, C.P., Principato, M.S., Erba, E., Corselli, C., 2008. Synchronous basin-wide formation and redox-controlled preservation of a Mediterranean sapropel. Nature Geoscience 1, 606-610.
Favaretto, S., Asioli, A., Miola, A., Piva, A., 2008. Preboreal climatic oscillations recorded by pollen and foraminifera in the southern Adriatic Sea. Quaternary International 190, 89-102.
Filippidi, A., Triantaphyllou, M.V., De Lange, G.J., 2016. Eastern-Mediterranean ventilation variability during sapropel S1 formation, evaluated at two sites influenced by deep-water formation from Adriatic and Aegean Seas. Quaternary Science Reviews 144, 95-106.
Giunta, S., Negri, A., Morigi, C., Capotondi, L., Combourieu-Nebout, N., Emeis, K., Sangiorgi, F., Vigliotti, L., 2003. Coccolithophorid ecostratigraphy and multi-proxy paleoceanographic reconstruction in the Southern Adriatic Sea during the last deglacial time (Core AD91-17). Palaeogeography, Palaeoclimatology, Palaeoecology 190, 39-59.
Gogou, A., Bouloubassi, I., Lykousis, V., Arnaboldi, M., Gaitani, P., Meyers, P.A., 2007. Organic geochemical evidence of Late Glacial–Holocene climate instability in the North Aegean Sea. Palaeogeography, Palaeoclimatology, Palaeoecology 256, 1-20.

769 Gordon, E.S., Goñi, M.A., 2003. Sources and distribution of terrigenous organic matter delivered by the
770 Atchafalaya River to sediments in the northern Gulf of Mexico. Geochimica et Cosmochimica Acta 67,
771 2359-2375.
772 Grimm, R., Maier-Reimer, E., Mikolajewicz, U., Schmiedl, G., Müller-Navarra, K., Adloff, F., Grant, K.M.,
773 Ziegler, M., Lourens, L.J., Emeis, K.-C., 2015. Late glacial initiation of Holocene eastern Mediterranean
774 sapropel formation. Nature communications 6.
775 Hennekam, R., Jilbert, T., Schnetger, B., Lange, G.J., 2014. Solar forcing of Nile discharge and sapropel S1
776 formation in the early to middle Holocene eastern Mediterranean. Paleoceanography 29, 343-356.
777 Hilgen, F., 1991. Astronomical calibration of Gauss to Matuyama sapropels in the Mediterranean and
778 implication for the geomagnetic polarity time scale. Earth and planetary science letters 104, 226-244.
779 Jorissen, F.J., 1988. Benthic foraminifera from the Adriatic Sea: principles of phenotypic variation.
780 Utrecht Micropaleontological Bulletins 37.
781 Jorissen, F.J., 1999. Benthic foraminiferal successions across Late Quaternary Mediterranean sapropels.
782 Marine Geology 153, 91-101.
783 Jorissen, F.J., Asioli, A., Borsetti, A., Capotondi, L., De Visser, J., Hilgen, F., Rohling, E., Van der Borg, K.,
784 Grazzini, C.V., Zachariasse, W., 1993. Late quaternary central Mediterranean biochronology. Marine
785 Micropaleontology 21, 169-189.
786 Klein, B., Roether, W., Civitarese, G., Gacic, M., Manca, B.B., d'Alcala, M.R., 2000. Is the Adriatic returning
787 to dominate the production of Eastern Mediterranean Deep Water. Geophys. Res. Lett 27, 3377-3380.
788 Kotthoff, U., Pross, J., Müller, U.C., Peyron, O., Schmiedl, G., Schulz, H., Bordon, A., 2008. Climate
789 dynamics in the borderlands of the Aegean Sea during formation of sapropel S1 deduced from a marine
790 pollen record. Quaternary Science Reviews 27, 832-845.
791 Langgut, D., Almogi-Labin, A., Bar-Matthews, M., Weinstein-Evron, M., 2011. Vegetation and climate
792 changes in the South Eastern Mediterranean during the Last Glacial-Interglacial cycle (86 ka): new marine
793 pollen record. Quaternary Science Reviews 30, 3960-3972.
794 Langone, L., Conese, I., Miserocchi, S., Boldrin, A., Bonaldo, D., Carniel, S., Chiggiato, J., Turchetto, M.,
795 Borghini, M., Tesi, T., 2015. Dynamics of particles along the western margin of the Southern Adriatic:
796 Processes involved in transferring particulate matter to the deep basin. Marine Geology.
797 Lowe, J.J., Blockley, S., Trincardi, F., Asioli, A., Cattaneo, A., Matthews, I.P., Pollard, M., Wulf, S., 2007.
798 Age modelling of late Quaternary marine sequences in the Adriatic: Towards improved precision and
799 accuracy using volcanic event stratigraphy. Continental Shelf Research 27, 560-582.
800 Magny, M., Combourieu-Nebout, N., De Beaulieu, J., Bout-Roumazeilles, V., Colombaroli, D., Desprat, S.,
801 Francke, A., Joannin, S., Peyron, O., Revel, M., 2013. North-south palaeohydrological contrasts in the
802 central Mediterranean during the Holocene: tentative synthesis and working hypotheses. Climate of the
803 Past Discussions 9, 1901-1967 (IF 1903,1509).
804 Magny, M., Joannin, S., Galop, D., Vannière, B., Haas, J.N., Bassetti, M., Bellintani, P., Scandolari, R.,
805 Desmet, M., 2012. Holocene palaeohydrological changes in the northern Mediterranean borderlands as
806 reflected by the lake-level record of Lake Ledro, northeastern Italy. Quaternary Research 77, 382-396.
807 Marchini, G., Zanchetta, G., Santacroce, R., Vigliotti, L., Capotondi, L., Sulpizio, R., 2014.
808 Tephrostratigraphy of marine core AD91-17 (Adriatic Sea) Revised. Alpine and Mediterranean
809 Quaternary 27, 77-84.
810 Marini, M., Maselli, V., Campanelli, A., Foglini, F., Grilli, F., 2015. Role of the Mid-Adriatic deep in dense
811 water interception and modification. Marine Geology.
812 Marino, G., Rohling, E.J., Sangiorgi, F., Hayes, A., Casford, J.L., Lotter, A.F., Kucera, M., Brinkhuis, H., 2009.
813 Early and middle Holocene in the Aegean Sea: interplay between high and low latitude climate
814 variability. Quaternary Science Reviews 28, 3246-3262.
815 McCave, I., Hall, I.R., 2006. Size sorting in marine muds: Processes, pitfalls, and prospects for
816 paleoflow-speed proxies. Geochemistry, Geophysics, Geosystems 7.

Mercone, D., Thomson, J., Abu-Zied, R., Croudace, I., Rohling, E., 2001. High-resolution geochemical and micropalaeontological profiling of the most recent eastern Mediterranean sapropel. Marine Geology 177, 25-44.
Mercone, D., Thomson, J., Croudace, I., Siani, G., Paterne, M., Troelstra, S., 2000. Duration of S1, the most recent sapropel in the eastern Mediterranean Sea, as indicated by accelerator mass spectrometry radiocarbon and geochemical evidence. Paleoceanography 15, 336-347.
Millot, C., 1999. Circulation in the western Mediterranean Sea. Journal of Marine Systems 20, 423-442.
Minisini, D., Trincardi, F., Asioli, A., 2006. Evidence of slope instability in the Southwestern Adriatic Margin. Natural Hazards and Earth System Science 6, 1-20.
Möbius, J., Lahajnar, N., Emeis, K.-C., 2010. Diagenetic control of nitrogen isotope ratios in Holocene sapropels and recent sediments from the Eastern Mediterranean Sea. Biogeosciences 7, 3901-3914.
Narciso, Á., Flores, J.-A., Cachão, M., Piva, A., Asioli, A., Andersen, N., Schneider, R., 2012. Late Glacial–Holocene transition in the southern Adriatic Sea: Coccolithophore and Foraminiferal evidence. micropaleontology, 523-538.
Nieuwenhuize, J., Maas, Y.E.M., Middelburg, J.J., 1994. Rapid analysis of organic carbon and nitrogen in particulate materials. Marine Chemistry 45, 217-224.
Nijenhuis, I., Schenau, S., Van der Weijden, C., Hilgen, F., Lourens, L., Zachariasse, W., 1996. On the origin of upper Miocene sapropelites: a case study from the Faneromeni section, Crete (Greece). Paleoceanography 11, 633-645.
Passier, H.F., Middelburg, J.J., de Lange, G.J., Böttcher, M.E., 1997. Pyrite contents, microtextures, and sulfur isotopes in relation to formation of the youngest eastern Mediterranean sapropel. Geology 25, 519-522.
Piva, A., 2007. Stratigrafia ad alta risoluzione dei depositi Quaternari in Adriatico centrale e meridionale:impatto di cambiamenti climatici a scala sub-Milankoviana sulla circolazione in Mediterraneo, University of Bologna. Bologna, Bologna.
Piva, A., Asioli, A., Trincardi, F., Schneider, R.R., Vigliotti, L., 2008. Late-Holocene climate variability in the Adriatic sea (Central Mediterranean). The Holocene 18, 153-167.
Ramsey, C.B., 1995. Radiocarbon calibration and analysis of stratigraphy; the OxCal program. Radiocarbon 37, 425-430.
Ramsey, C.B., Lee, S., 2013. Recent and planned developments of the program OxCal. Radiocarbon 55, 720-730.
Reimer, P.J., Bard, E., Bayliss, A., Beck, J.W., Blackwell, P.G., Bronk Ramsey, C., Buck, C.E., Cheng, H., Edwards, R.L., Friedrich, M., 2013. IntCal13 and Marine13 radiocarbon age calibration curves 0-50,000 years cal BP.
Reitz, A., Thomson, J., de Lange, G.J., Hensen, C., 2006. Source and development of large manganese enrichments above eastern Mediterranean sapropel S1. Paleoceanography 21.
Rogerson, M., Cacho, I., Jimenez-Espejo, F., Reguera, M.I., Sierro, F.J., Martinez-Ruiz, F., Frigola, J., Canals, M., 2008. A dynamic explanation for the origin of the western Mediterranean organic-rich layers. Geochemistry, Geophysics, Geosystems 9, n/a-n/a.
Rohling, E., Bryden, H., 1994. Estimating past changes in the Eastern Mediterranean freshwater budget, using reconstructions of sea level and hydrography. Proceedings of the Koninklijke Nederlandse Akademie van Wetenschappen 97, 201-217.
Rohling, E., Jorissen, F., De Stigter, H., 1997. 200 year interruption of Holocene sapropel formation in the Adriatic Sea. Journal of Micropalaeontology 16, 97-108.
Rohling, E., Marino, G., Grant, K., 2015. Mediterranean climate and oceanography, and the periodic development of anoxic events (sapropels). Earth-Science Reviews 143, 62-97.
Rossignol-Strick, M., 1985. Mediterranean Quaternary sapropels, an immediate response of the African monsoon to variation of insolation. Palaeogeography, palaeoclimatology, palaeoecology 49, 237-263.

Rossignol-Strick, M., Nesteroff, W., Olive, P., Vergnaud-Grazzini, C., 1982. After the deluge: Mediterranean stagnation and sapropel formation.
Sachs, J.P., Repeta, D.J., 1999. Oligotrophy and nitrogen fixation during eastern Mediterranean sapropel events. Science 286, 2485-2488.
Sangiorgi, F., Capotondi, L., Combourieu Nebout, N., Vigliotti, L., Brinkhuis, H., Giunta, S., Lotter, A.F., Morigi, C., Negri, A., Reichart, G.J., 2003. Holocene seasonal sea-surface temperature variations in the southern Adriatic Sea inferred from a multiproxy approach. Journal of Quaternary Science 18, 723-732.
Santacroce, R., Cioni, R., Marianelli, P., Sbrana, A., Sulpizio, R., Zanchetta, G., Donahue, D.J., Joron, J.L., 2008. Age and whole rock–glass compositions of proximal pyroclastics from the major explosive eruptions of Somma-Vesuvius: a review as a tool for distal tephrostratigraphy. Journal of Volcanology and Geothermal Research 177, 1-18.
Santvoort, P., Lange, G., Langereis, C., Dekkers, M., Paterne, M., 1997. Geochemical and paleomagnetic evidence for the occurrence of “missing” sapropels in eastern Mediterranean sediments. Paleoceanography 12, 773-786.
Schmiedl, G., Kuhnt, T., Ehrmann, W., Emeis, K.-C., Hamann, Y., Kotthoff, U., Dulski, P., Pross, J., 2010. Climatic forcing of eastern Mediterranean deep-water formation and benthic ecosystems during the past 22 000 years. Quaternary Science Reviews 29, 3006-3020.
Schmiedl, G., Mitschele, A., Beck, S., Emeis, K.-C., Hemleben, C., Schulz, H., Sperling, M., Weldeab, S., 2003. Benthic foraminiferal record of ecosystem variability in the eastern Mediterranean Sea during times of sapropel S 5 and S 6 deposition. Palaeogeography, Palaeoclimatology, Palaeoecology 190, 139-164.
Siani, G., Magny, M., Paterne, M., Debret, M., Fontugne, M., 2013. Paleohydrology reconstruction and Holocene climate variability in the South Adriatic Sea. Climate of the Past 9, 499-515.
Siani, G., Paterne, M., Arnold, M., Bard, E., Métivier, B., Tisnerat, N., Bassinot, F., 2000. Radiocarbon reservoir ages in the Mediterranean Sea and Black Sea. Radiocarbon 42, 271-280.
Siani, G., Paterne, M., Colin, C., 2010. Late glacial to Holocene planktic foraminifera bioevents and climatic record in the South Adriatic Sea. Journal of Quaternary Science 25, 808-821.
Spagnoli, F., Dell'Anno, A., De Marco, A., Dinelli, E., Fabiano, M., Gadaleta, M.V., Ianni, C., Loiacono, F., Manini, E., Marini, M., 2010. Biogeochemistry, grain size and mineralogy of the central and southern Adriatic Sea sediments: a review. Chemistry and Ecology 26, 19-44.
Spötl, C., Nicolussi, K., Patzelt, G., Boch, R., 2010. Humid climate during deposition of sapropel 1 in the Mediterranean Sea: Assessing the influence on the Alps. Global and Planetary Change 71, 242-248.
Tachikawa, K., Vidal, L., Cornuault, M., Garcia, M., Pothin, A., Sonzogni, C., Bard, E., Menot, G., Revel, M., 2015. Eastern Mediterranean Sea circulation inferred from the conditions of S1 sapropel deposition. Clim. Past 11, 855-867.
Tesi, T., Langone, L., Goni, M., Turchetto, M., Miserocchi, S., Boldrin, A., 2008. Source and composition of organic matter in the Bari canyon (Italy): dense water cascading versus particulate export from the upper ocean. Deep Sea Research Part I: Oceanographic Research Papers 55, 813-831.
Tesi, T., Miserocchi, S., Goni, M.e.a., Langone, L., Boldrin, A., Turchetto, M., 2007. Organic matter origin and distribution in suspended particulate materials and surficial sediments from the western Adriatic Sea (Italy). Estuarine, Coastal and Shelf Science 73, 431-446.
Tesi, T., Semiletov, I., Hugelius, G., Dudarev, O., Kuhry, P., Gustafsson, Ö., 2014. Composition and fate of terrigenous organic matter along the Arctic land–ocean continuum in East Siberia: Insights from biomarkers and carbon isotopes. Geochimica et Cosmochimica Acta 133, 235-256.
Toucanne, S., Minto'o, C.M.A., Fontanier, C., Bassetti, M.-A., Jorry, S.J., Jouet, G., 2015. Tracking rainfall in the northern Mediterranean borderlands during sapropel deposition. Quaternary Science Reviews 129, 178-195.

Trincardi, F., Cattaneo, A., Asioli, A., Correggiari, A., Langone, L., 1996. Stratigraphy of the late-Quaternary deposits in the central Adriatic basin and the record of short-term climatic events. MEMORIE-ISTITUTO ITALIANO DI IDROBIOLOGIA 55, 39-70.

Trincardi, F., Verdicchio, G., Miserocchi, S., 2007. Seafloor evidence for the interaction between cascading and along-slope bottom water masses. Journal of Geophysical Research: Earth Surface 112.

Turchetto, M., Boldrin, A., Langone, L., Miserocchi, S., Tesi, T., Foglini, F., 2007. Particle transport in the Bari canyon (southern Adriatic Sea). Marine Geology 246, 231-247.

Van Straaten, L., 1970. Holocene and late-Pleistocene sedimentation in the Adriatic Sea. Geologische Rundschau 60, 106-131.

Versteegh, G.J.M., Zonneveld, K.A.F., de Lange, G.J., 2010. Selective aerobic and anaerobic degradation of lipids and palynomorphs in the Eastern Mediterranean since the onset of sapropel S1 deposition. Marine Geology 278, 177-192.

Vigliotti, L., Asioli, A., Bergami, C., Capotondi, L., Piva, A., 2011. Magnetic properties of the youngest sapropel S1 in the Ionian and Adriatic Sea: inference for the timing and mechanism of sapropel formation. Italian journal of geosciences 130, 106-118.

Vigliotti, L., Verosub, K., Cattaneo, A., Trincardi, F., Asioli, A., Piva, A., 2008. Palaeomagnetic and rock magnetic analysis of Holocene deposits from the Adriatic Sea: detecting and dating short-term fluctuations in sediment supply. The Holocene 18, 141-152.

Vilibić, I., Orlić, M., 2002. Adriatic water masses, their rates of formation and transport through the Otranto Strait. Deep Sea Research Part I: Oceanographic Research Papers 49, 1321-1340.

Vilibić, I., Supić, N., 2005. Dense water generation on a shelf: the case of the Adriatic Sea. Ocean Dynamics 55, 403-415.

Weldeab, S., Menke, V., Schmiedl, G., 2014. The pace of East African monsoon evolution during the Holocene. Geophysical Research Letters 41, 1724-1732.

Zanchetta, G., Drysdale, R.N., Hellstrom, J.C., Fallick, A.E., Isola, I., Gagan, M.K., Pareschi, M.T., 2007. Enhanced rainfall in the Western Mediterranean during deposition of sapropel S1: stalagmite evidence from Corchia cave (Central Italy). Quaternary Science Reviews 26, 279-286.

Captions

Figure 1. Map of the study area in the Adriatic Sea. Coring sites are displayed as filled dots and labelled AMC99-1 (260 m water depth), SA03-1 (567 m water depth), INVAS12-10 (570 m water depth) and ST04-1 (1085 m water depth) respectively. Arrows show the main water masses which include the Levantine Intermediate Water (LIW, red, main path, and dashed red, northward intrusion with large inter-decadal variability), North ~~and South~~ Adriatic Deep Water (NAdDW ~~and SAdDW,~~, blue) and the Eastern Mediterranean Deep Water (EMDW, green). Dashed line roughly displays the position of the shoreline at the S1 onset. ~~The black line represents the location of the depth profile (Fig. 2a).~~ The upper right inset shows the main path of the LIW in the eastern and central Mediterranean Sea and the Nile runoff input

Figure 2. Chirp profiles of the coring sites along the shelf-basin continuum. (a) The depth profile graph displays the general location of the sediment cores in respect to the dominant water masses (NAdDW and LIW). Seismic profiles through the three coring sites: (b) shelf-adjacent (mid-Adriatic depression, AMC99-1), (c) slope (sediment wave field, SA03-1 and INVAS12-10) and (d) deep basin (ST04-1).

987
988
989
990
991
992
993
994
995
996
997
998
999
1000
1001
1002
1003
1004
1005
1006
1007
1008

Figure 3. Sediment cores from the Adriatic Sea (Fig. 1 and 2). Lithology, photo, false colours and XRAY of AMC99-1 (a), photo non available); INVAS12-10 (b); and ST04-1 (c).

Figure 4. Down-core biostratigraphy of ST04-1, SA03-1 and AMC99-1. Four bioevents were used for the age-depth model: I (top YD, blue line), II (older peak *G. inflata*, light green), III (younger peak *G. inflata*, dark green), IV (last occurrence *G. inflata*, red line). For further details on the bioevents see Table 1 and method section. The figure shows also the correlation between twins core Core SA03-1 and INVAS12-10. collected in the sediment wave field. Cross-correlation between twin cores relays on bioevents and tephra (magnetic susceptibility anomalies). Events in chronological order include: top of the Younger Dryas, two *Globorotalia inflata* peaks (during the Pre Boreal), peak of *Cassidulinoides bradyi*, a large magnetic susceptibility peak marking a tephra layer, two *G. inflata* peaks (during S1 break and S1b, respectively) and the last Occurrence of *G. inflata*

Figure 5. Bayesian age-depth model of Adriatic records (median, 1σ and 2σ). Filled symbols (circles, squares and diamonds) show the radiocarbon dates used for the Bayesian model. Dark gray areas display distinct bioevents used to increase the model resolution and synchronize the records. The model shows good agreement between bioevents and the new radiocarbon dates of monospecific tests. For further details about the age-depth model see the method section. The paleoceanographic (and stratigraphic) events were identified independently in each core; therefore, all dates in each core are consistent and independent as no age is exported from one core to another.

Figure 6. Comparison between sediment cores collected in the southern Adriatic basin. ST04-1 (this study), IN68-9 (Rohling et al., 1997), MD90-197 (Mercone et al., 2001; Siani et al., 2010) and AD90-17 (Capotondi et al., 1999). A) Location of the sediment cores. B) Core description, biostratrigraphy and

~~bioevents (coloured lines). C) Core description and V/Al ratio (MD90-197 vs ST04-1). Radiocarbon dates shown in the figure refer to uncalibrated data (^{14}C yBP) for a direct comparison.~~

Figure ~~7~~6. Sapropel S1 along the Adriatic shelf-basin continuum and external environmental forcings. Organic carbon (OC) content of (a) ST04-1, (b) INVAS12-10 and (c) AMC99-1. Note the different scale of y-axes. Bottom current ~~proxes~~proxies: abundance of reworked inner-shelf foraminifera (d) and sortable

silt (e) over the slope (SA03-1). (f) Nile runoff proxy: Ba/Ca of *Globigerinoides ruber* (Weldeab et al., 2014). Light and dark grey areas denote pre-sapropel sediments, ~~the~~ S1 boundaries and the sapropel S1 break based on the OC content of ST04-1.

Figure ~~8~~7. Seafloor oxygen content and reducing conditions during the sapropel S1 deposition in Adriatic sediment along the shelf-basin continuum. Foraminifera-based oxygen index (OI, (Schmiedl et al., 2010)

of (a) ST04-1, (b) SA03-01 and AMC99-1). Value of 1 refers to fully oxygenated conditions while 0 represents azoic environment, respectively. Note, OI of AMC99-1 is based on intermediate infaunal foraminifera. Authigenic vanadium enrichment (V/Ti) of (~~a~~d) ST04-1, (~~b~~e) SA03-01 and (f) AMC99-1. Light and dark grey areas show pre-sapropel sediments, ~~the~~ S1 boundaries and interruption based on the OC content of ST04-1 (see Fig. ~~1~~6).

Figure ~~98~~ 98. Pre-sapropel and sapropel S1 onset in the Adriatic basin (ST04-1, 1085 m). (a) Organic carbon (OC) and oxygen index. (b) Abundance of deep and intermediate infaunal foraminifera and authigenic vanadium enrichment (V/TiO_2). Light grey area shows the azoic environment.

Figure ~~10~~9. Distribution of manganese and sulfur during the S1 deposition in Adriatic sediments along the shelf-basin continuum. Authigenic manganese enrichment of (a) ST04-1, (b) INVAS12-10 and (c) AMC99-1. Authigenic sulfur enrichment of (d) ST04-1, (e) INVAS12-10 and (f) AMC99-1. Light and dark grey areas show pre-sapropel sediments, S1 boundaries and interruption based on the OC content of ST04-1 (see Fig. 6). ~~. Light and dark grey areas show the S1 boundaries and interruption based on the OC content (see Fig. 1).~~ Note the different scale of y-axes.

Figure 10. Benthic ecosystem changes over water depth during the sapropel S1 deposition according to the foraminifera-based oxygen index. Changes were defined using the oxygen index threshold according to Schmiedl et al. (2010). Values less than 0.5 indicate the collapse of the benthic ecosystem while values more than 0.5 indicate the recovery of the benthic ecosystem. Solid line and grey area show mean and standard deviation of the S1 onset, respectively. Dashed line (interpolation water depth *vs* time) exhibits the progressive ventilation with increasing water depth over time. Aegean and Levantine data from Schmiedl et al. (2010).

Figure ~~6~~11. Comparison between sediment cores collected in the southern Adriatic basin. ST04-1 (this study), IN68-9 (Rohling et al., 1997), MD90-197 (Mercone et al., 2001; Siani et al., 2010) and AD90-17 (Capotondi et al., 1999). A) Location of the sediment cores. B) Core description, biostratrigraphy and bioevents (coloured lines). C) Core description and V/Al ratio (MD90-197 vs ST04-1). Radiocarbon dates shown in the figure refer to uncalibrated data (^{14}C yBP) for a direct comparison.

Figure 12~~1~~. Terrigenous organic carbon concentration during the sapropel S1 deposition in Adriatic sediments along the shelf-basin continuum. Lignin concentration of (a) ST04-1, (b) INVAS12-10 and (c) AMC99-1~~. Light and dark grey areas show the S1 boundaries and interruption based on the OC content (see Fig. 1)~~. Light and dark grey areas show pre-sapropel sediments, S1 boundaries and interruption based on the OC content of ST04-1 (see Fig. 6).~~.~~ Note the different scale of y-axes.

~~**Figure 12.** Cartoon of the thermohaline circulation: (a) modern conditions and (b) during the freshening of the Eastern Mediterranean Sea via the Nile (b). As the precipitation increases over North Africa, the Levantine Intermediate Waters (LIW) progressively decreases. This is turn hampers the preconditioning North Adriatic Deep Water with cascade effects on the Eastern Mediterranean Deep Water formation. The expression of the monsoon-fuelled freshening was a synchronous S1 formation across the Eastern Mediterranean Sea including the Adriatic.~~

Table S1. Dated levels used for the Bayesian age-depth model of core AMC991, INVAS12-10, ST04-1. The table contains a new radiocarbon date of core IN68-9 as well.

Lab. #	Core depth (cm)	Sample type	^{14}C age (yBP)	Modelled age (median, cal yBP)	-2δ	+2δ	Reference
AMC99-1 (260 m w.d.)							
Poz-16133	21-22	*Cibicidoides pachyderma*	1405 ± 30	629	720	530	Piva et al. (2008)
Poz-16134	117-118	*Cibicidoides pachyderma*	2880 ± 40	2208	2331	2073	Piva et al. (2008)
Poz-16135	222-223	*Cibicidoides pachyderma*	4200 ± 40	3889	4065	3724	Piva et al. (2008)
Poz-16137	258-259	mixed planktic	4570 ± 50	4630	4798	4464	Piva et al. (2008)
CAMS-33373	323-324	mixed planktic	5880 ± 60	6104	6265	5944	Bioevent IV, LO *G. inflata* (core RF93-30); (Trincardi et al., 1996)
OS-104703	374-375.5	*Globigerinoides ruber*	6720 ± 50	7046	7201	6906	this study
OS-104710	416-417	*Globigerinoides ruber*	7320 ± 60	7668	7805	7553	this study
OS-104283	470-471.5	*Globigerinoides ruber*	8230 ± 45	8565	8721	8420	this study
OS-104466	535-536	*Globigerinoides ruber*	9090 ± 35	9683	9856	9533	this study
Poz-16142	550-551	mixed planktic	9360 ± 50	10049	10184	9886	Bioevent III, Younger peak *G. inflata* (core SA03-1); (Favaretto et al., 2008)
Poz-16144	570-571	mixed planktic	9860 ± 60	10565	10727	10392	Bioevent II, Older peak *G. inflata* (core SA03-1); (Favaretto et al., 2008)
CAMS-16305	610-611	mixed planktic	10450 ± 90	11301	11623	11112	Bioevent I, Top YD (core CM92-43); (Asioli et al., 2001)
INVAS12-10 (570 m w.d.)							
CAMS-33373	275-276	mixed planktic	5880 ± 60	6116	6277	5937	Bioevent IV, LO *G. inflata* (core RF93-30); (Trincardi et al., 1996)
OS-104282	305-306	*Globigerinoides ruber*	6450 ± 35	6833	7115	6647	this study
OS-104380	319-320	*Globigerinoides ruber*	7340 ± 30	7648	7760	7558	this study
OS-108068	327-328	*Globigerinoides ruber*	7530 ± 60	7864	7986	7725	this study
OS-104381	347-348	*Globigerinoides ruber*	8240 ± 35	8565	8721	8421	this study

OS-104382	375-376	*Globigerinoides ruber*	9140 ± 35	9596	9982	9151	this study
Poz-16142	389-390	mixed planktic	9360 ± 50	10100	10232	9885	Bioevent III, Younger peak *G. inflata* (core SA03-1); (Favaretto et al., 2008)
Poz-16144	395-396	mixed planktic	9860 ± 60	10577	10768	10373	Bioevent II, Older peak *G. inflata* (core SA03-1); (Favaretto et al., 2008)
CAMS-16305	413-414	mixed planktic	10450 ± 90	11301	11682	11088	Bioevent I, Top YD (core CM92-43); (Asioli et al., 2001)
ST04-1 (1085 m w.d.)							
CAMS-33373	80-81	mixed planktic	5880 ± 60	6103	6275	5925	Bioevent IV, LO *G. inflata* (core RF93-30); (Trincardi et al., 1996)
OS-104464	102-103	*Globigerinoides ruber*	6510 ± 30	6878	7011	6735	this study
OS-104378	113-114	*Globigerinoides ruber*	7160 ± 30	7521	7607	7425	this study
OS-104465	120-121	*Globigerinoides ruber*	7800 ± 35	8110	8254	7985	this study
OS-104281	139-140	*Globigerinoides ruber*	9040 ± 40	9562	9701	9455	this study
OS-107637	142-143	*Globigerinoides ruber*	9180 ± 40	9755	9916	9580	this study
Poz-16142	145-146	mixed planktic	9360 ± 50	10009	10181	9826	Bioevent III, Younger peak *G. inflata* (core SA03-1); (Favaretto et al., 2008)
Poz-16144	153-154	mixed planktic	9860 ± 60	10669	10842	10505	Bioevent II, Older peak *G. inflata* (core SA03-1); (Favaretto et al., 2008)
OS-104379	154-155	*Globorotalia inflata*	10050 ± 45	10761	10949	10624	this study
CAMS-16305	169-170	mixed planktic	10450 ± 90	11442	11790	11165	Bioevent I, Top YD (core CM92-43); (Asioli et al., 2001)
~~**IN68-9 (1234 m w.d.)**~~							
~~OS-127850~~	~~137-138~~	~~*Globigerinoides ruber*~~	~~9030 ± 30~~	~~Not calibrated for direct comparison with previous studies Rohling et al. (1997)~~			

* For further details about biostratigraphy and bioevents see the method section in the main text

1244

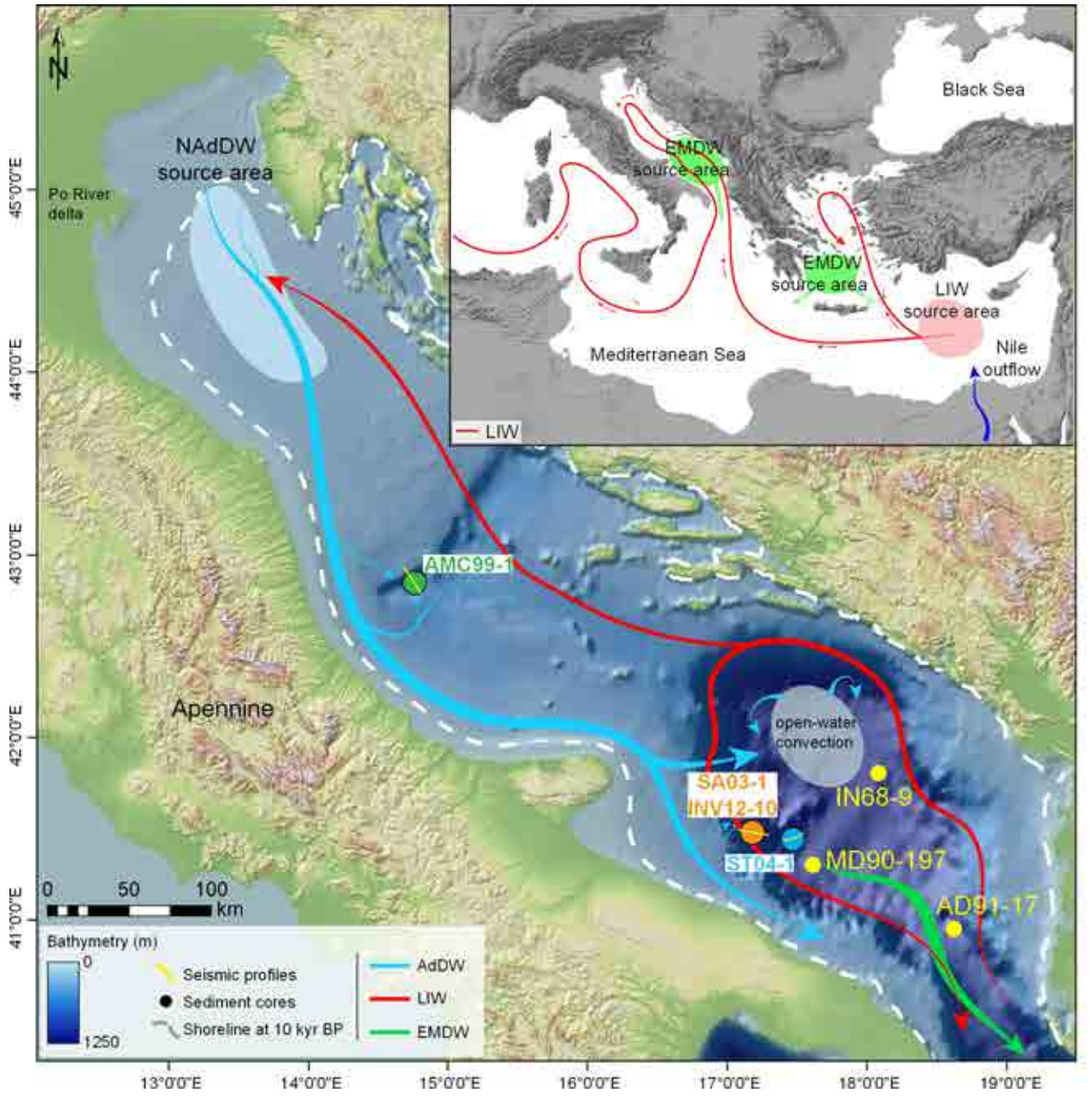
NAdDW
source area
Po River
delta
Apennine
AMC99-1
SA03-1
INV12-10
ST04-1
IN68-9
MD90-197
AD91-17
open-water
convection
Black Sea
EMDW
source area
EMDW
source area
LIW
source area
Mediterranean Sea
Nile
outflow
LIW
0
50
100
km
Bathymetry (m)
0
1250
Seismic profiles
Sediment cores
Shoreline at 10 kyr BP
AdDW
LIW
EMDW
45°0'0"E
44°0'0"E
43°0'0"E
42°0'0"E
41°0'0"E
13°0'0"E
14°0'0"E
15°0'0"E
16°0'0"E
17°0'0"E
18°0'0"E
19°0'0"E

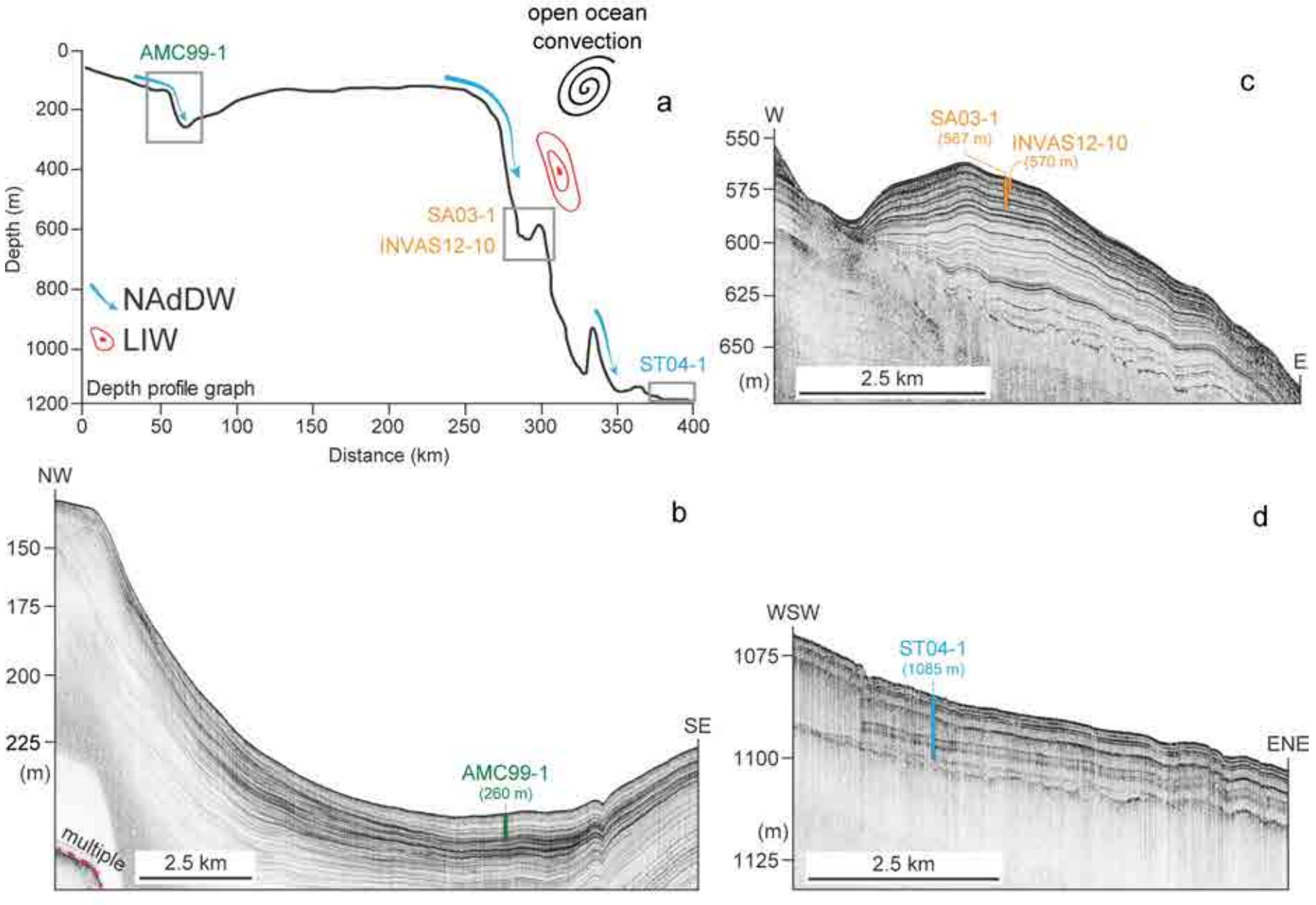
open ocean
convection
a
AMC99-1
SA03-1
INVAS12-10
ST04-1
NAdDW
LIW
Depth profile graph
Depth (m)
Distance (km)
0
200
400
600
800
1000
1200
0
50
100
150
200
250
300
350
400
c
W
SA03-1
(567 m)
INVAS12-10
(570 m)
550
575
600
625
650
(m)
2.5 km
E
NW
b
150
175
200
225
(m)
SE
AMC99-1
(260 m)
multiple
2.5 km
d
WSW
ST04-1
(1085 m)
1075
1100
(m)
1125
ENE
2.5 km

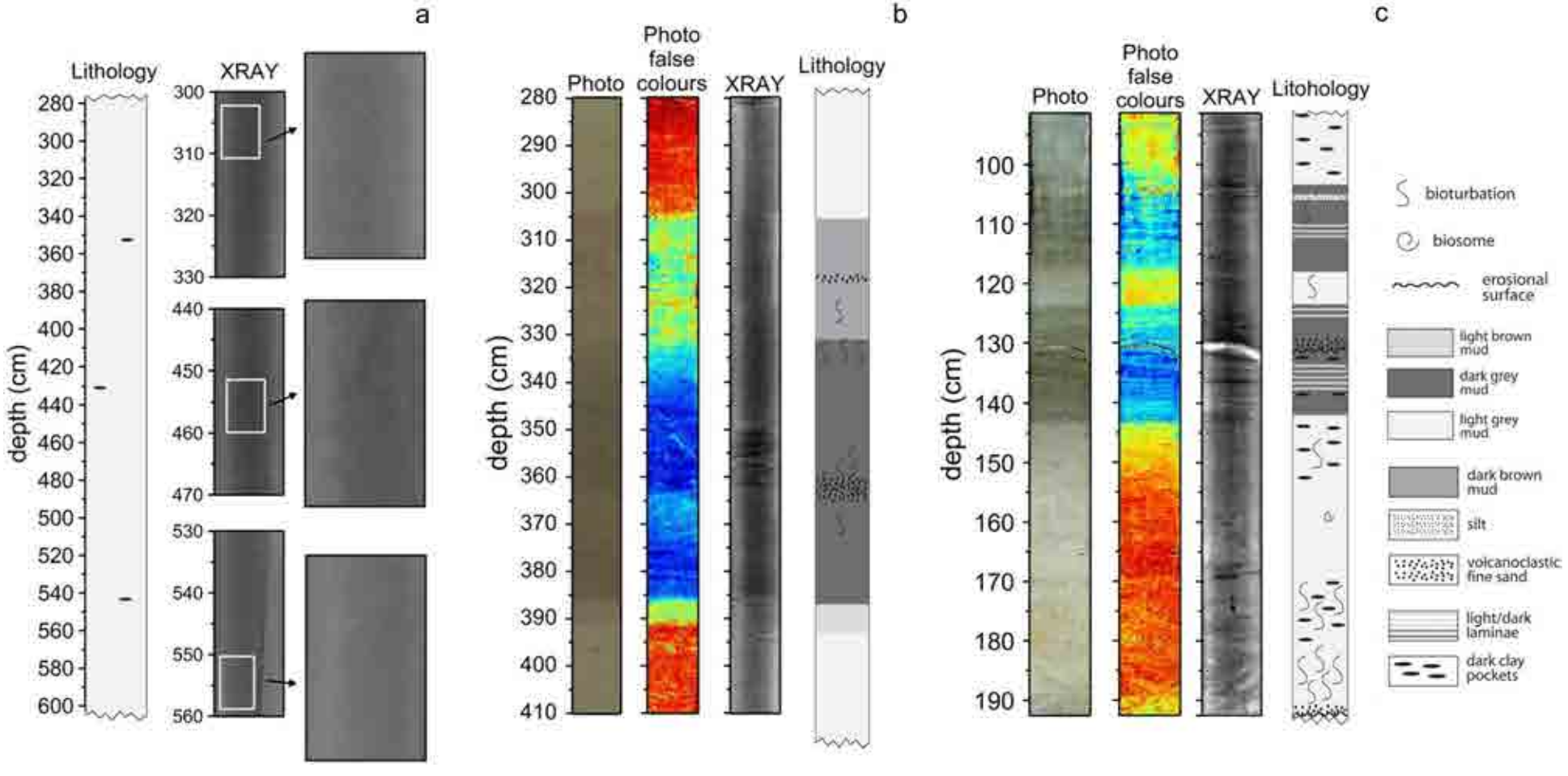
core AMC99-1 (260 m)
a
Lithology
XRAY
depth (cm)
core INVAS12-10 (570 m)
b
Photo
Photo false colours
XRAY
Lithology
depth (cm)
core ST04-1 (1085 m)
c
Photo
Photo false colours
XRAY
Litohology
depth (cm)
bioturbation
biosome
erosional surface
light brown mud
dark grey mud
light grey mud
dark brown mud
silt
volcanoclastic fine sand
light/dark laminae
dark clay pockets

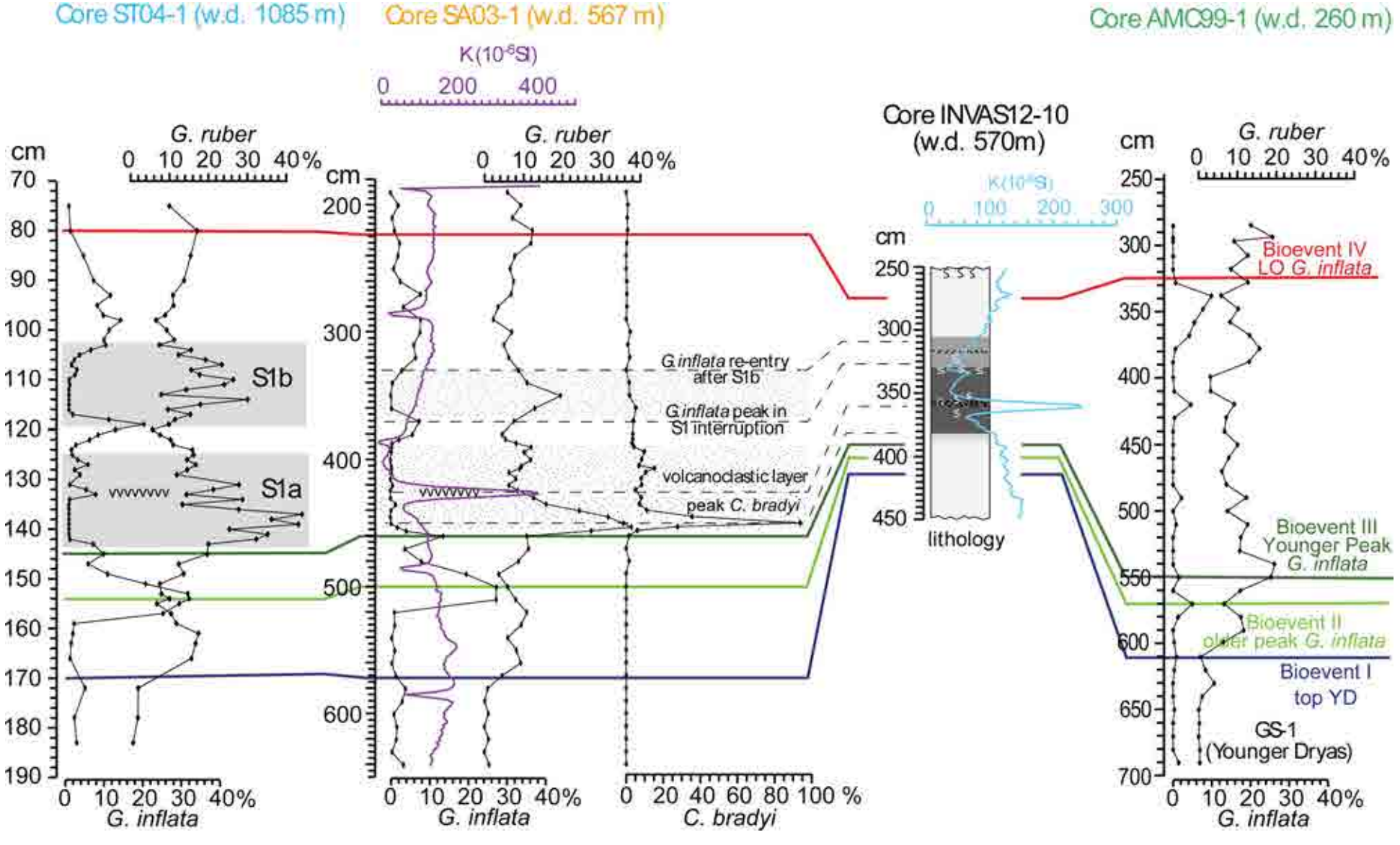
Core ST04-1 (w.d. 1085 m)
Core SA03-1 (w.d. 567 m)
Core AMC99-1 (w.d. 260 m)
K(10⁻⁶SI)
0 200 400
Core INVAS12-10
(w.d. 570m)
K(10⁻⁶SI)
0 100 200 300
G. ruber
0 10 20 30 40%
cm
S1b
S1a
G.inflata re-entry after S1b
G.inflata peak in S1 interruption
volcanoclastic layer
peak C. bradyi
lithology
Bioevent IV
LO G. inflata
Bioevent III
Younger Peak
G. inflata
Bioevent II
older peak G. inflata
Bioevent I
top YD
GS-1
(Younger Dryas)
G. inflata
0 10 20 30 40%
C. bradyi
0 20 40 60 80 100 %

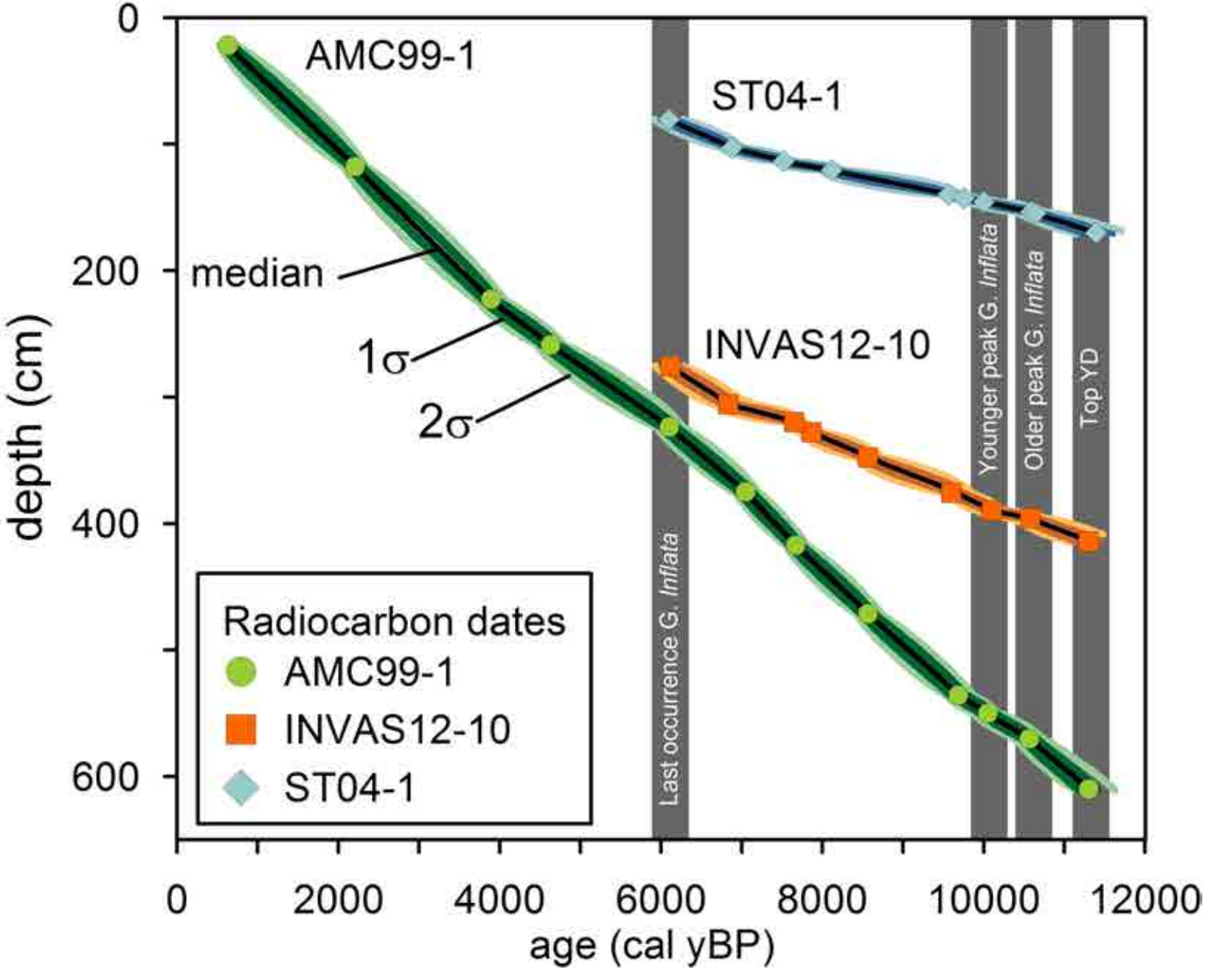
AMC99-1
ST04-1
INVAS12-10
median
1σ
2σ
Last occurrence G. Inflata
Younger peak G. Inflata
Older peak G. Inflata
Top YD
Radiocarbon dates
AMC99-1
INVAS12-10
ST04-1
depth (cm)
0
200
400
600
0
2000
4000
6000
8000
10000
12000
age (cal yBP)

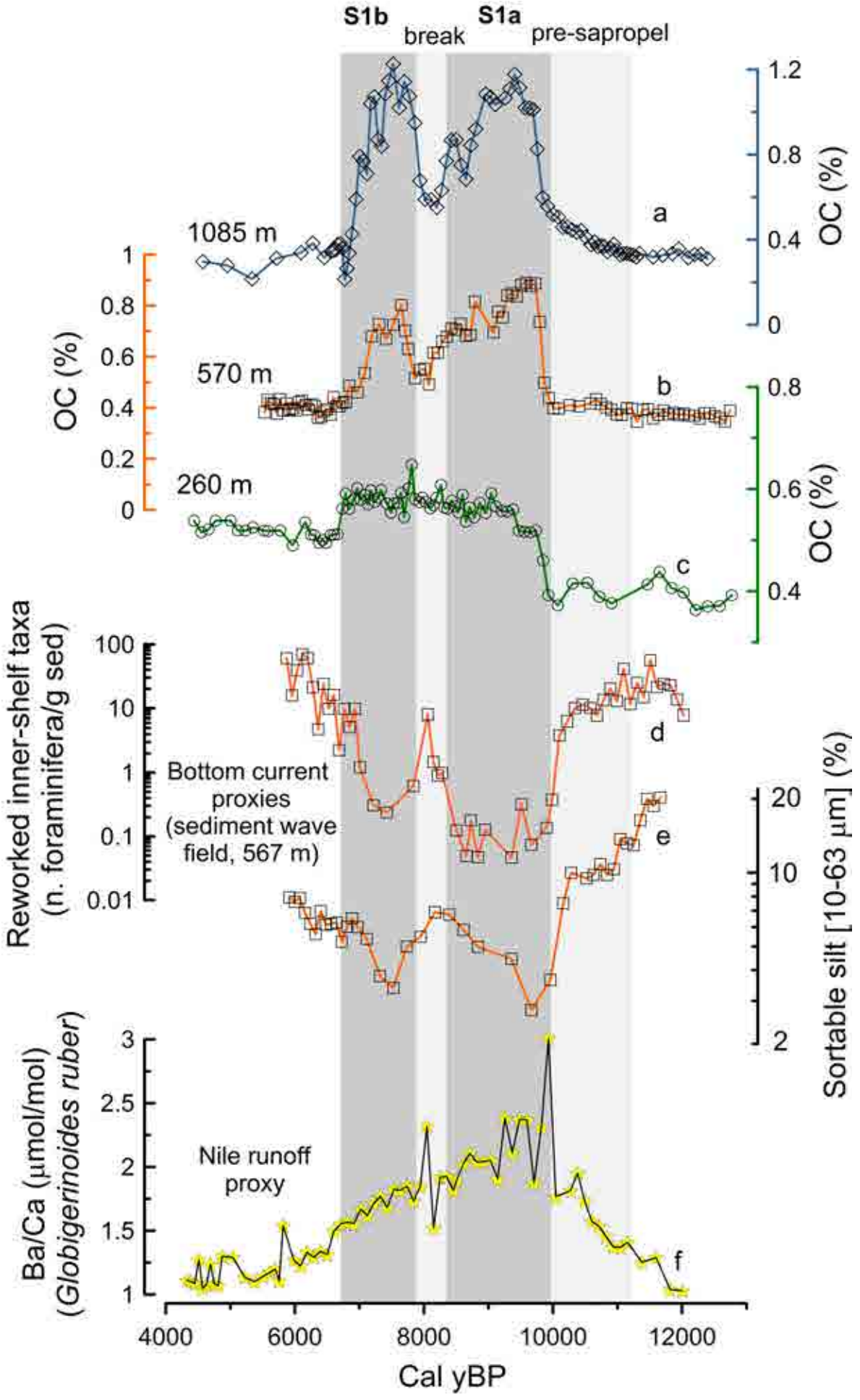
S1b
break
S1a
pre-sapropel
1085 m
570 m
260 m
a
b
c
OC (%)
OC (%)
OC (%)
Reworked inner-shelf taxa
(n. foraminifera/g sed)
Bottom current
proxies
(sediment wave
field, 567 m)
d
e
Sortable silt [10-63 µm] (%)
Ba/Ca (µmol/mol)
(Globigerinoides ruber)
Nile runoff
proxy
f
Cal yBP

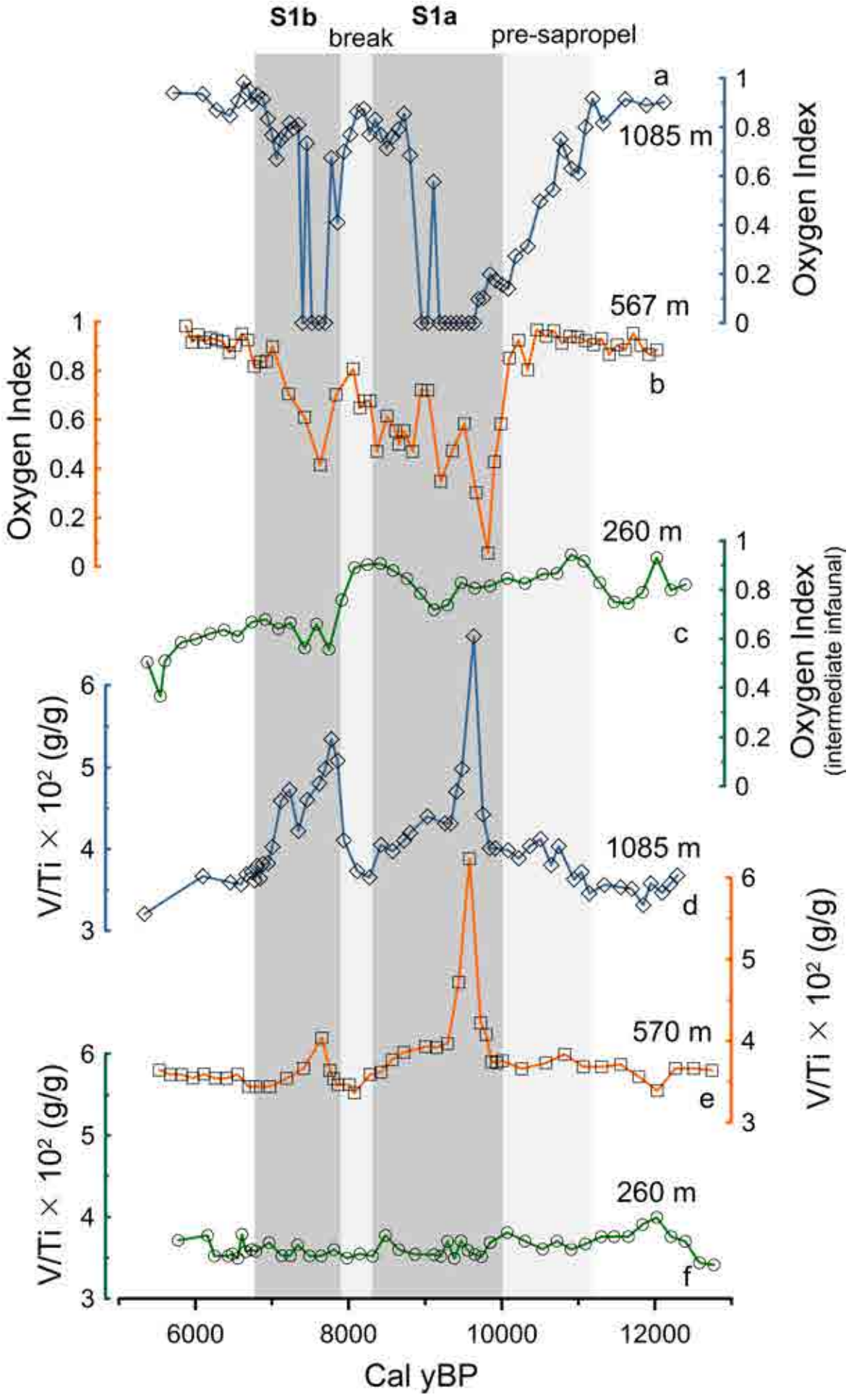
S1b
break
S1a
pre-sapropel
a
1085 m
Oxygen Index
567 m
b
Oxygen Index
260 m
c
Oxygen Index
(intermediate infaunal)
V/Ti × 10² (g/g)
1085 m
d
570 m
e
V/Ti × 10² (g/g)
V/Ti × 10² (g/g)
260 m
f
6000
8000
10000
12000
Cal yBP

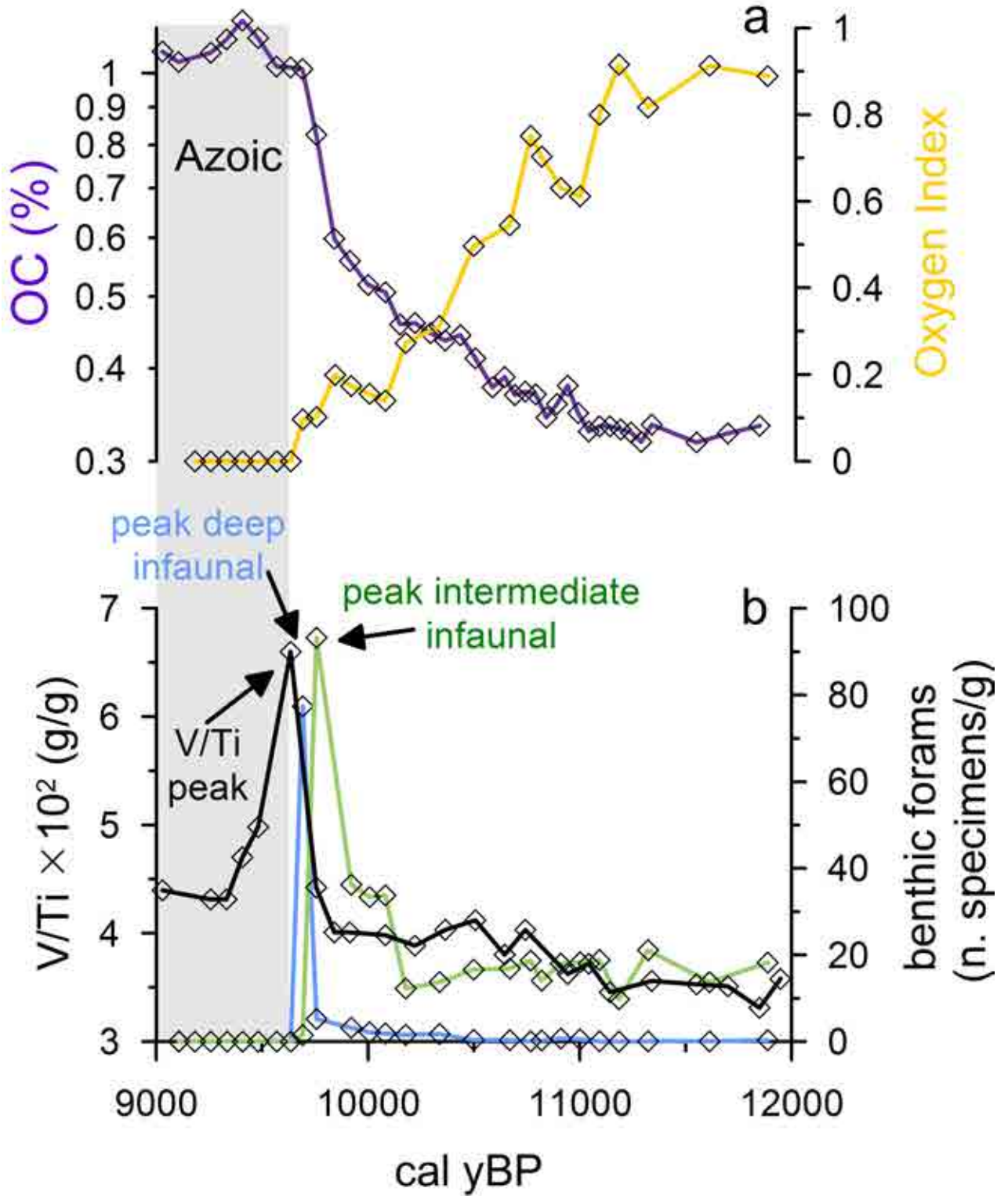
core ST04-1 (1085 m)
a
b
OC (%)
Oxygen Index
Azoic
peak deep infaunal
peak intermediate infaunal
V/Ti peak
V/Ti ×10² (g/g)
benthic forams (n. specimens/g)
cal yBP
9000
10000
11000
12000

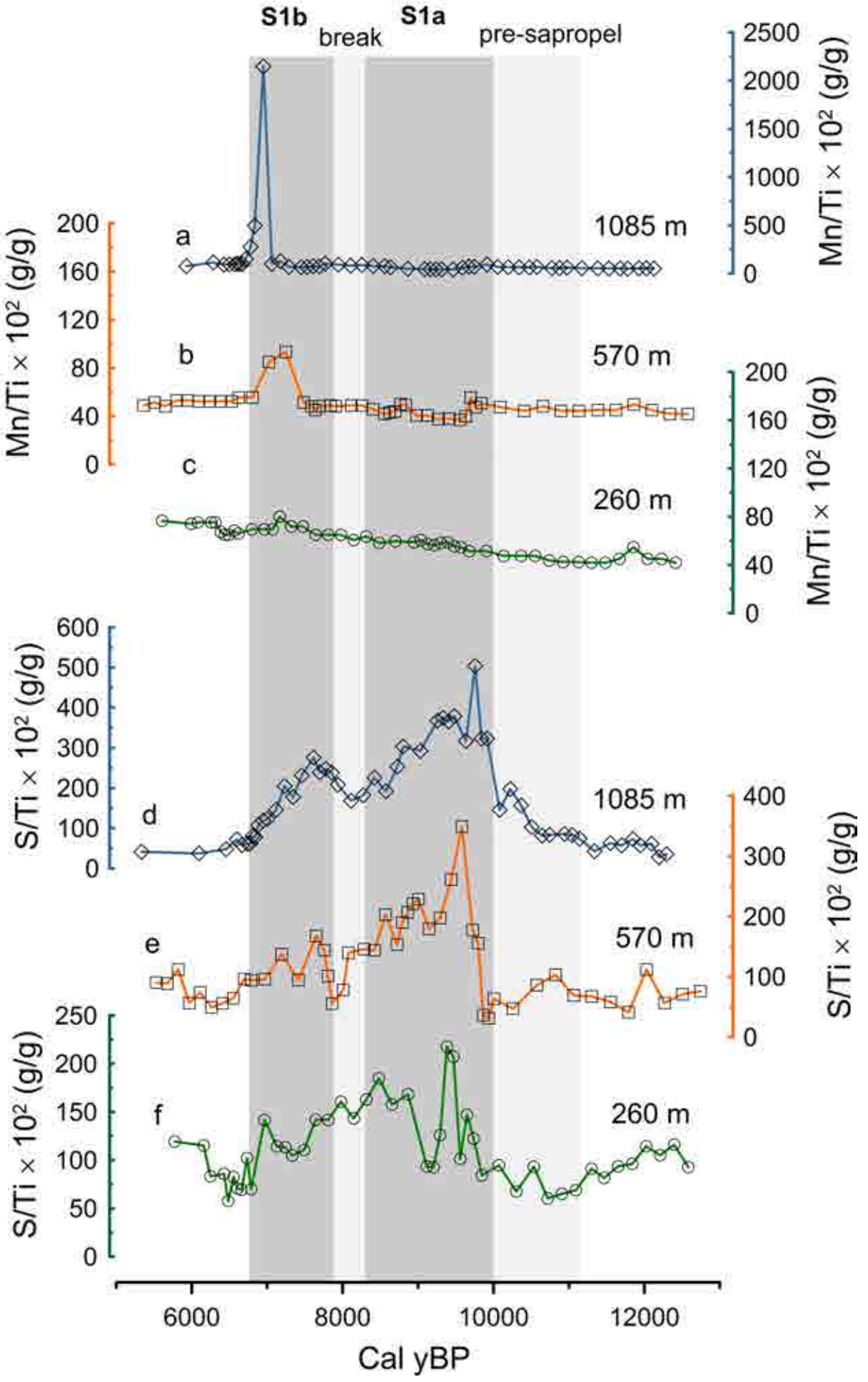
S1b
break
S1a
pre-sapropel
a
1085 m
b
570 m
c
260 m
d
1085 m
e
570 m
f
260 m
Mn/Ti × 10² (g/g)
S/Ti × 10² (g/g)
Cal yBP
6000
8000
10000
12000

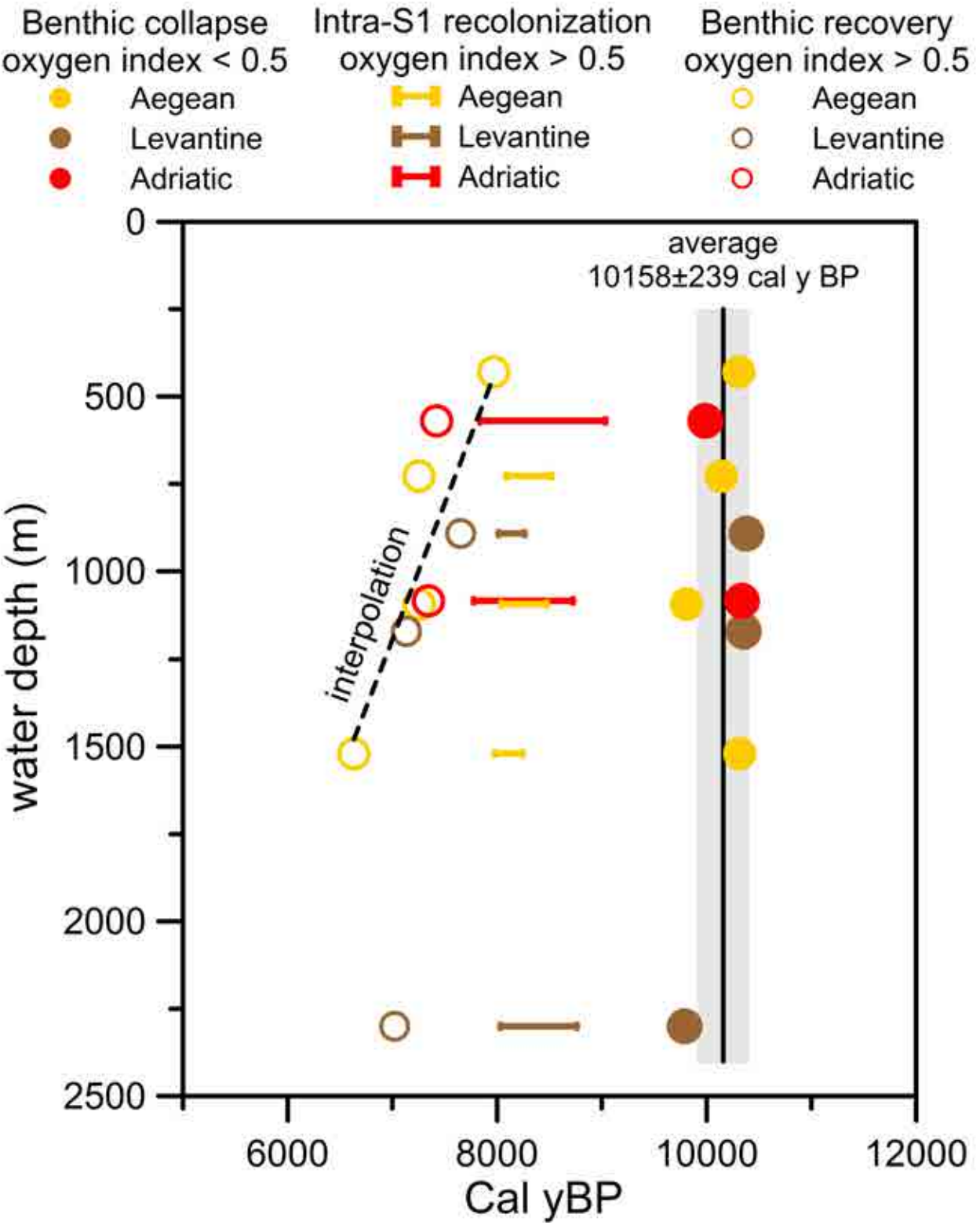
Benthic collapse
oxygen index < 0.5
Aegean
Levantine
Adriatic
Intra-S1 recolonization
oxygen index > 0.5
Aegean
Levantine
Adriatic
Benthic recovery
oxygen index > 0.5
Aegean
Levantine
Adriatic
average
10158±239 cal y BP
interpolation
water depth (m)
0
500
1000
1500
2000
2500
6000
8000
10000
12000
Cal yBP

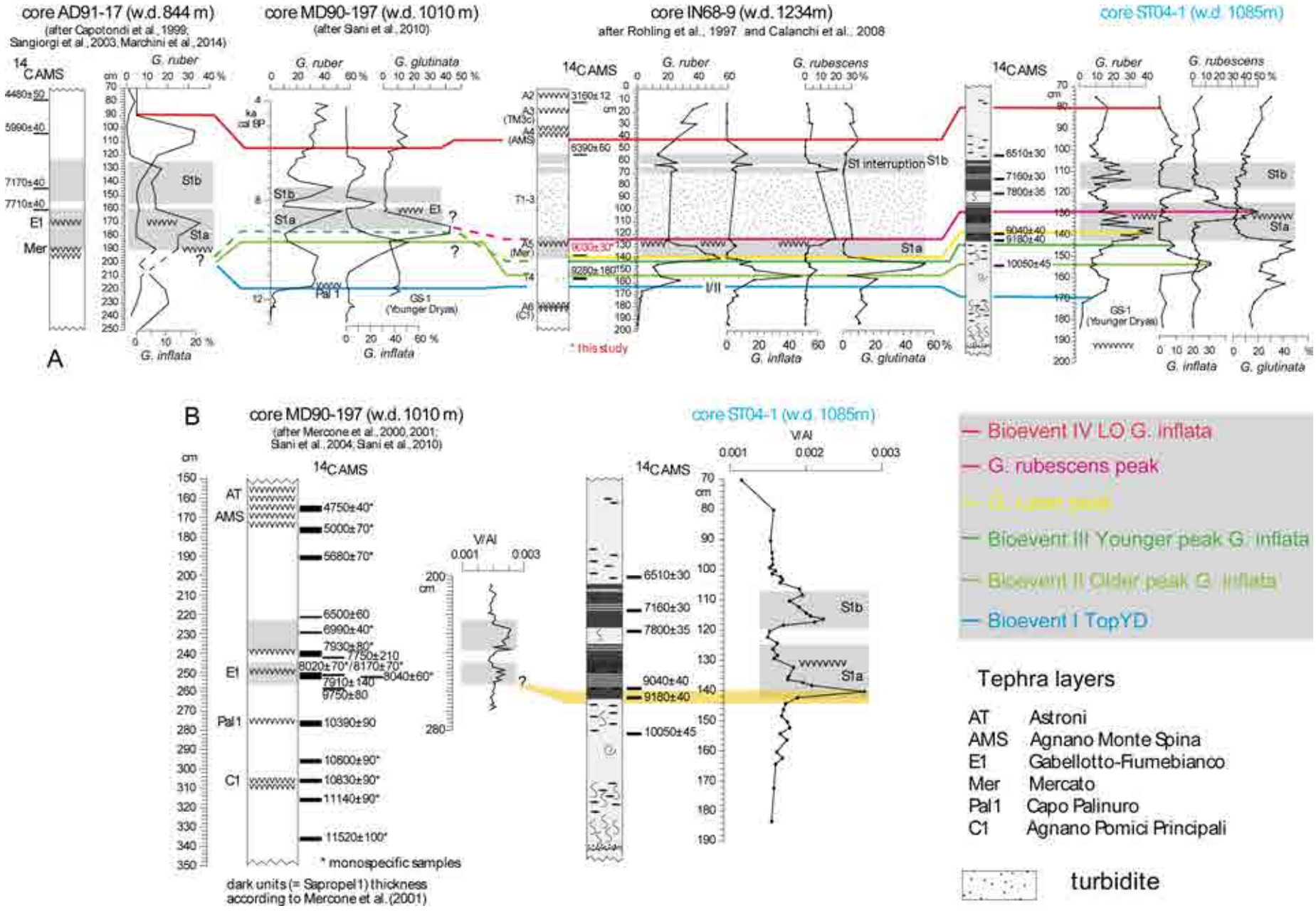
core AD91-17 (w.d. 844 m)
(after Capotondi et al., 1999; Sangiorgi et al., 2003; Marchini et al., 2014)
core MD90-197 (w.d. 1010 m)
(after Siani et al., 2010)
core IN68-9 (w.d. 1234m)
after Rohling et al., 1997 and Calanchi et al., 2008
core ST04-1 (w.d. 1085m)
14CAMS
G. ruber
G. glutinata
G. rubescens
G. inflata
S1b
S1a
E1
Mer
Pal 1
GS-1 (Younger Dryas)
S1 interruption
T1-3
T2
T4
T5
A2
A3 (TM3c)
A4 (AMS)
A6 (C1)
I/II
* this study
A
B
core MD90-197 (w.d. 1010 m)
(after Mercone et al., 2000, 2001; Siani et al., 2004; Siani et al., 2010)
core ST04-1 (w.d. 1085m)
V/Al
AT
AMS
E1
Pal1
C1
4750±40*
5000±70*
5680±70*
6500±60
6990±40*
7930±80*
7750±210
8020±70*/8170±70*
8040±60*
7910±140
9750±80
10390±90
10600±90*
10830±50*
11140±90*
11520±100*
* monospecific samples
dark units (= Sapropel 1) thickness according to Mercone et al. (2001)
6510±30
7160±30
7800±35
9040±40
9180±40
10050±45
Bioevent IV LO G. inflata
G. rubescens peak
G. ruber peak
Bioevent III Younger peak G. inflata
Bioevent II Older peak G. inflata
Bioevent I TopYD
Tephra layers
AT Astroni
AMS Agnano Monte Spina
E1 Gabellotto-Fiumebianco
Mer Mercato
Pal1 Capo Palinuro
C1 Agnano Pomici Principali
turbidite

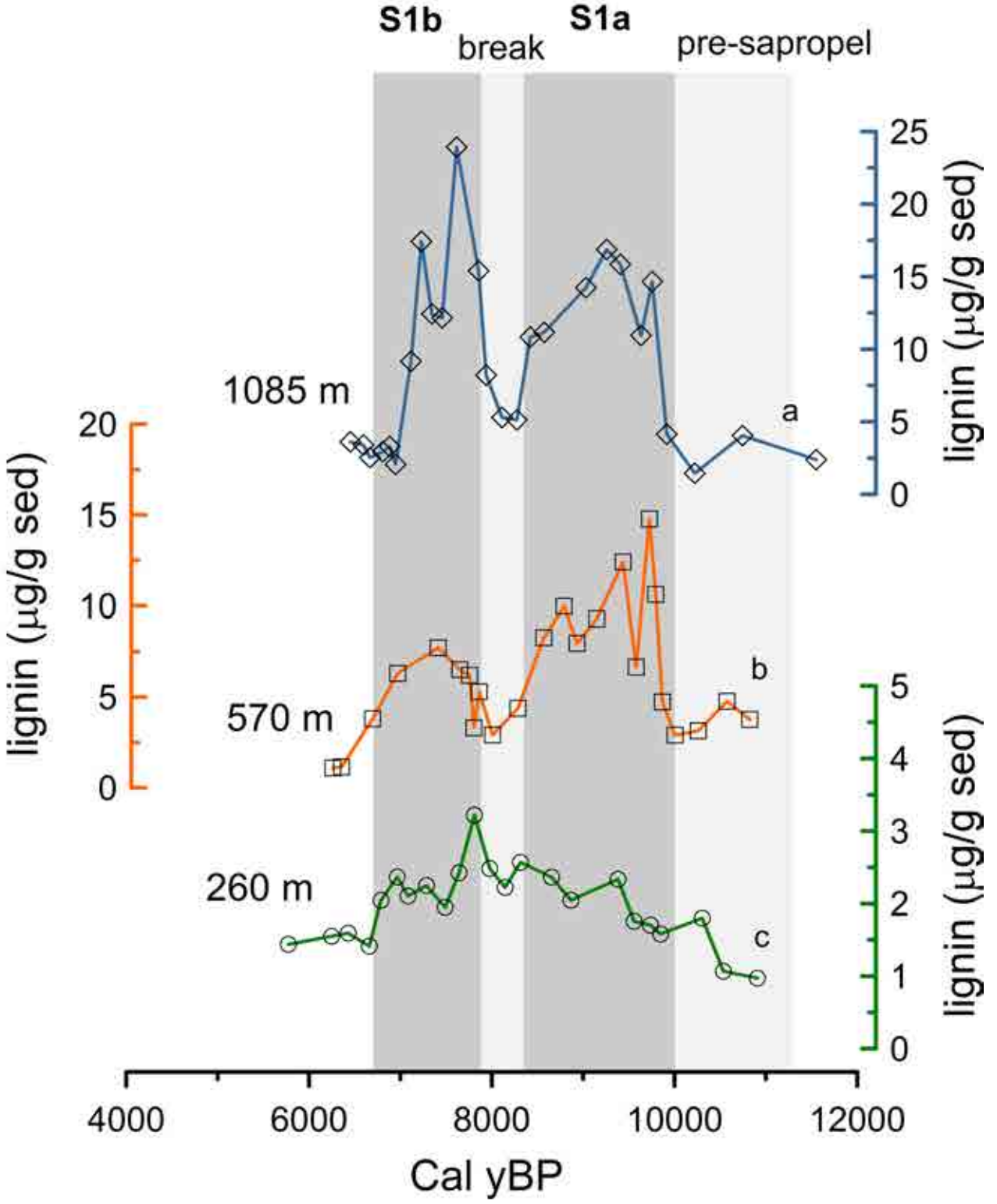
S1b
break
S1a
pre-sapropel
1085 m
570 m
260 m
a
b
c
lignin (µg/g sed)
lignin (µg/g sed)
lignin (µg/g sed)
0
5
10
15
20
0
5
10
15
20
25
0
1
2
3
4
5
4000
6000
8000
10000
12000
Cal yBP

In this section, we revisit the age-depth model originally presented by Rohling et al. (1997) using Oxcal. The new model allows for random fluctuations in sediment deposition (P_sequence) and benefits of a new radiocarbon date (monospecific planktonic test, *G. ruber*, reference OS-127850) (Table S1). In addition to the radiocarbon tests, the model relays on well-characterized, radiocarbon dated bioevents (I,II, III, IV) as specified in the main text and Table S1. Our overarching goal is to understand whether the offset (ca. 1ky) between our results and Rohling et al. (1997) is a consequence of the age-depth model constrain. The Oxcal script used to generate the model is reported below. Particular attention was given to the agreement index which measures the coherence between the model (prior) and the observational data (likelihood).

Radiocarbon test UTC-501 (Table 1; Fig. S1,S2,S3) turned out having a low agreement index (ca. 4%) (Fig. S3) and thus considered as an outlier. Altogether, our analysis revealed that the offset derives from this radiocarbon value being relatively young.

Table S1. Radiocarbon dates of core IN68-9

Lab. #	depth (cm)	Sample	^{14}C age (yr BP)	Source
UTC-500	11.5	benthic forams	3160 ± 120	Rohling et al. (1997)
CAMS-33373	43	mixed planktic	5880 ± 60	Bioevent IV, LO G. inflata (core RF93-30); Trincardi et al. (1996)
UTC-1607	54.5	mixed planktic	6390 ± 60	Rohling et al. (1997)
OS-127850	137.5	*Globigerinoides ruber*	9030 ± 30	this study
Poz-16142	143	mixed planktic	9360 ± 50	Bioevent III, Younger peak G. inflata (core SA03-1); Favaretto et al. (2008)
Poz-16144	155	mixed planktic	9860 ± 60	Bioevent II, Older peak G. inflata (core SA03-1); Favaretto et al. (2008)
UTC-501	156.5	benthic forams	9280 ± 180	Rohling et al. (1997)
CAMS-16305	162.5	mixed planktic	10450 ± 90	Bioevent I, Top YD (core CM92-43); Asioli et al. (2001)
UTC-502	241.5	mixed planktic	13100 ± 200	Rohling et al. (1997)

Oxcal script

```
Options()
 {
  BCAD=FALSE;
 };
 Plot()
 {
  Curve("Marine13","Marine13.14c");
  Delta_R("DeltaR based on Calib", 136, 41);


P_Sequence("variable", 1,1,U(-2,2))

   {

Boundary("bottom")

   {

    z=242;

   };

R_Date("IN68-9 241.5", 13100,200)

{

z=241.5;

};

R_Date("BIO I", 10450,90)

{

z=162.5;

};

R_Date("IN68-9", 9280,180)

{

z=156.5;

};

R_Date("BIO II", 9860,60)

{

z=155;

};
```

```
R_Date("BIO III", 9360,50)

{

z=143; };

R_Date("IN68-9  137.5", 9030,30)

{

z=137.5; };

R_Date("IN68-9 54.5", 6390,60)

{

z=54.5; };

R_Date("BIO IV", 5880,60)

{

z=43;

};

R_Date("IN68-9 10.5",3160,120)

{

z=11.5;

};


Boundary();

  };
  };
 };
```

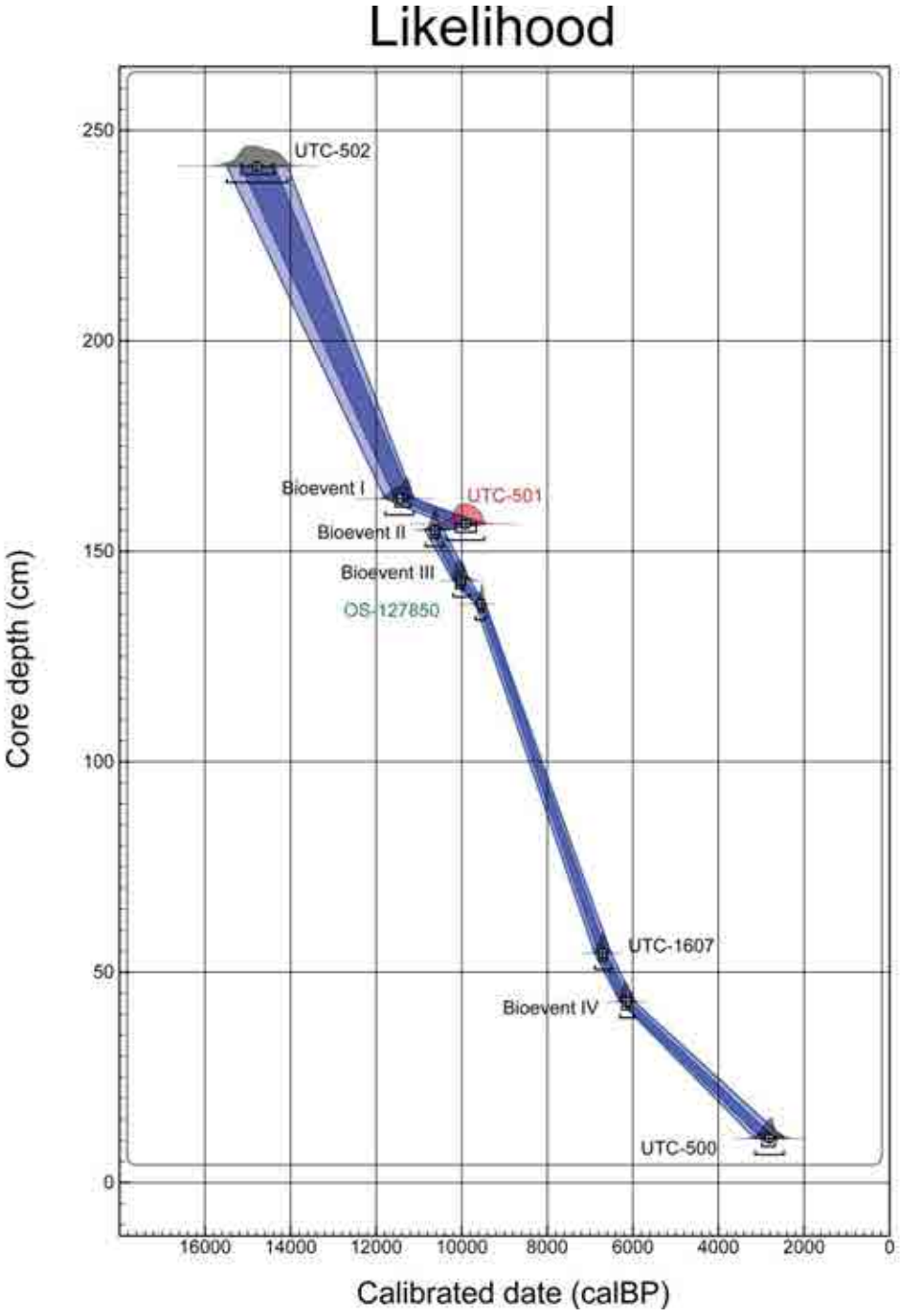

Fig. S1. Likelihood probability distributions of calibrated radiocarbon dates Light and dark blue show 1σ and 2σ, respectively.

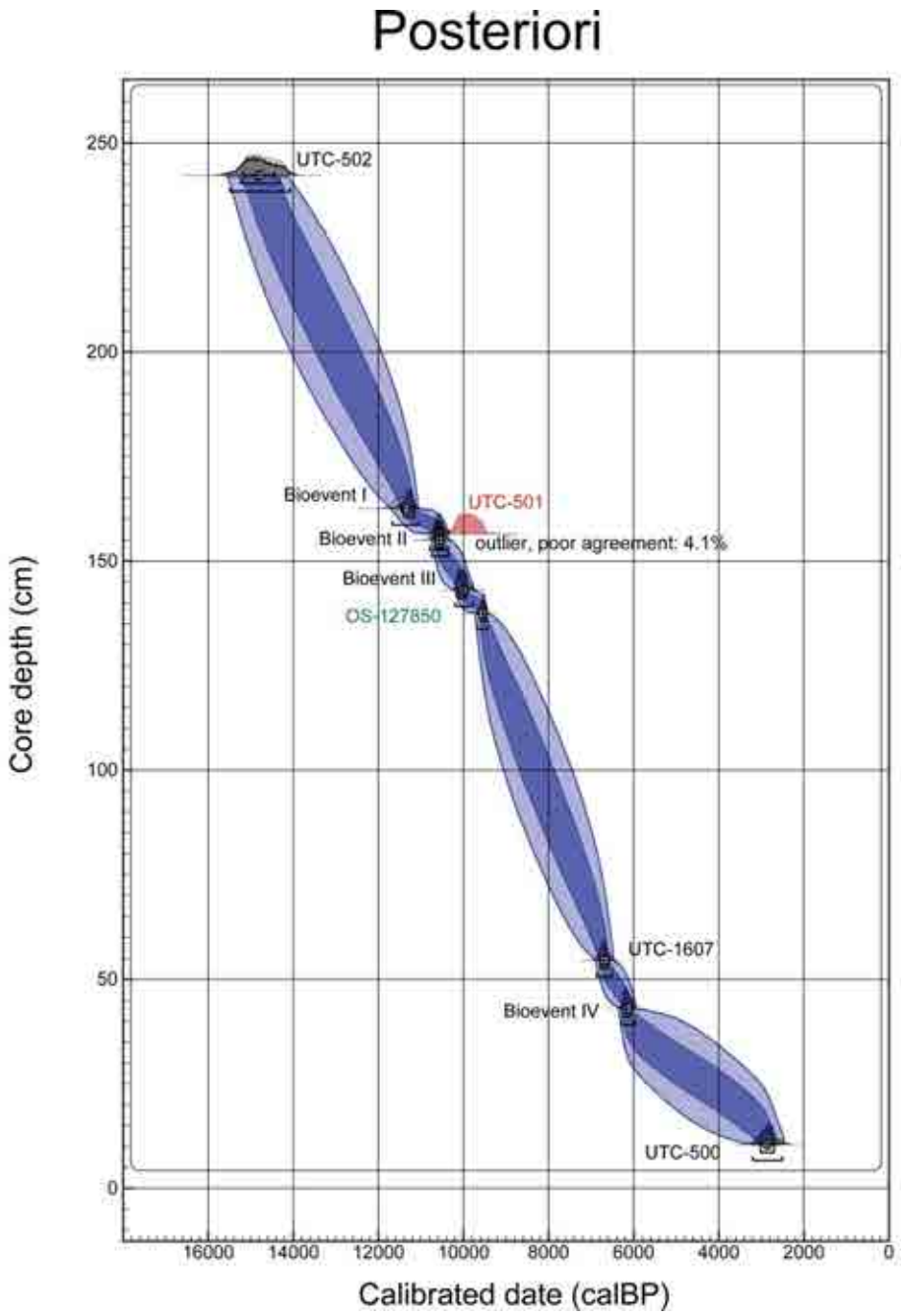

Fig. S2. Posterior probability distributions of calibrated radiocarbon dates Light and dark blue show 1σ and 2σ, respectively

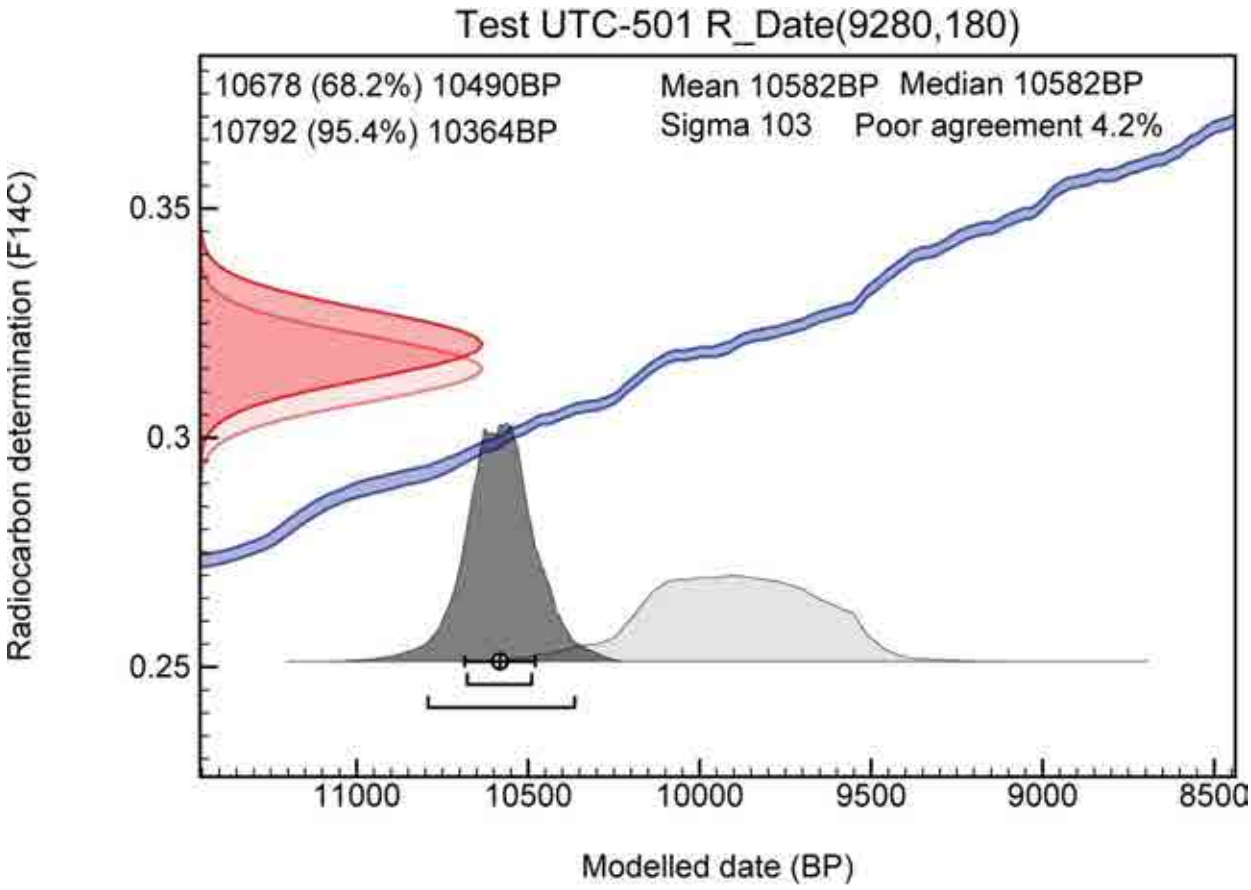

Fig. S3. Posterior probability distribution (dark grey) *vs* likelihood probability distribution (light gray) of test UTC-501.

Asioli, A., Trincardi, F., Lowe, J., Ariztegui, D., Langone, L., Oldfield, F., 2001. Sub-millennial scale climatic oscillations in the central Adriatic during the Lateglacial: palaeoceanographic implications. Quaternary Science Reviews 20, 1201-1221.

Favaretto, S., Asioli, A., Miola, A., Piva, A., 2008. Preboreal climatic oscillations recorded by pollen and foraminifera in the southern Adriatic Sea. Quaternary International 190, 89-102.

Rohling, E., Jorissen, F., De Stigter, H., 1997. 200 year interruption of Holocene sapropel formation in the Adriatic Sea. Journal of Micropalaeontology 16, 97-108.

Trincardi, F., Cattaneo, A., Asioli, A., Correggiari, A., Langone, L., 1996. Stratigraphy of the late-Quaternary deposits in the central Adriatic basin and the record of short-term climatic events. MEMORIE-ISTITUTO ITALIANO DI IDROBIOLOGIA 55, 39-70.

The Adriatic S1 is coeval with the Eastern Mediterranean S1 deposits

The Adriatic S1 onset is synchronous with the shutdown of the NAdDW

African monsoons weakened the LIW which in turn hampered the NAdDW formation